Accurate lifetime measurements using confocal microscopy

Patrik Brynolfsson

Master of Science Thesis

Laser Physics
Department of Applied Physics
School of Engineering Science
KTH

Stockholm, Sweden 2007

TRITA-FYS: 2007:15
ISSN: 0280-316X
ISRN: KTH/FYS/- -07:15- -SE

Abstract

In this master thesis a method for reducing radiation trapping by using a confocal microscope has been tested and analyzed, and theory to explain the results has been developed. Two types of numerical simulations, including a Monte Carlo simulation, have been constructed and analyzed to gain knowledge and understanding of the processes at work. The simulation results show that by using a confocal microscope the radiation trapping can be reduced significantly, if the set-up is properly designed. Further, an attempt to simulate the energy transfer in Er-Yb doped double-tungstate crystals using a Monte Carlo simulation has been made. The results were inconclusive, however, further work should easily correct the problem.

Sammanfattning

I detta examensarbete utvecklades en metod för att minska effekten av ”radiation trapping” genom att använda ett konfokalmikroskop, och teori för att förklara resultaten har tagits fram. Två olika numeriska simuleringar, inklusive en Monte Carlo-simulering, har utförts och analyserats för att öka förståelsen av de processer som sker. Resultaten av simuleringarna visar att man genom att använda ett konfokalmikroskop kan reducera ”radiation trapping” avsevärt, om de använda uppställningarna är rätt konstruerade. Ett försök att simulera energiöverföringar mellan Er och Yb-joner i kristall med en Monte Carlo-simulering gjordes också. Resultaten var ofullständiga, men med fortsatt arbete kan de felen lätt korrigeras.

Acknowledgements

First I would like to thank my supervisor, Stefan Bjurshagen for guiding me through this thesis project and explaining theory and experiments to me. Thanks also to my other supervisor, Valdas Pasiskevicius, for the necessary help down in the lab, as well as sharing your wisdom when needed, it is nice to know someone has all the answers! I am also grateful to my examiner, Professor Fredrik Laurell, for inviting me into his research group and giving me the opportunity to do my thesis project here, thank you! Thanks Per Jelger, Björn Jakobsson, Sandra Johansson, Carlotta Canalias, Jonas Hellström, Stefan Holmgren and Mikael Tiihonen for all your help down in the lab, and for taking the time to explain the things I did not understand, as well as helping me find all the components I needed in the lab jungle. Mats, thank you for all your advice, interesting discussions and good conversations, I will miss it! Finally, thank you Ida, for encouraging and inspiring me when I most needed it, and for all your ideas and suggestions. Thank you for helping me with your graphical expertise and sharing your experience, your help has been invaluable!

Contents

1 Introduction

Lasers are finding more and more applications in widely different areas of science and engineering, from scanning data off a CD or DVD to cutting and welding in heavy industries to analyzing the compositions of chemical compounds in bio-medical labs. This expansion causes a demand for tailored laser systems with strict specifications of size, output power, laser wavelength and beam quality. To meet these demands, a wide range of laser sources have been developed: gas lasers, solid-state lasers, free-electron lasers, dye lasers, diode lasers, x-ray plasma lasers etc., each with characteristics desirable in certain situations. The advent of the diode laser allowed lasers to be easily integrated in electronic devices, and would also provide a very suitable pump source for solid-state lasers. It was now possible to construct lasers with the desired properties of both these techniques: stable, compact, durable lasers with a wide choice of wavelengths and a good beam quality.

Er-doped solid-state lasers are used to generate laser light in the eye-safe region around 1.5 μm. Light at wavelengths above 1.4 μm are considered eye-safe, since it is absorbed in the eye before it hits the retina where it will cause permanent damage. This property makes these lasers ideal for applications in e.g. communication and range finding. In this thesis, crystals to be used in diode-pumped solid-state lasers have been examined in order to determine key characteristics such as lifetimes of energy levels and optimum doping concentrations. Improvements in terms of doping concentrations and design can be made by knowing the lifetimes of the different energy levels and understanding the dynamics in the laser system. By being able to simulate these processes, better crystal can be designed for specific applications with demands on power and size. In the work progress a certain measurement error became apparent when measuring the lifetimes of Er and Yb co-doped crystals, known as *radiation trapping*. When measuring lifetimes of energy levels, the intensity decay of the fluorescence emitted by atoms that change their energy state will serve as a clock. The faster the fluorescence intensity decay, the shorter the lifetime of the initial energy level in the atom. However, if the fluorescence is re-absorbed by other atoms in the crystal before it hits the detector, the fluorescence decay will seem slower than it really is, whereby measurements will indicate a longer lifetime of the energy level involved. This is known as radiation trapping. Radiation trapping can be very pronounced in quasi-three-level laser systems, such as Er and Yb atoms, since fluorescence is emitted as the atom decays to its ground state. This means that the radiation can also be *absorbed* by an atom in the ground state, of which there are plenty in the crystal.

The work conducted was then focused on methods of reducing this measurement error. This thesis can be divided into two distinct parts: constructing a method for reducing radiation trapping in the measurements,

and numerical simulations explaining and trying to replicate the results acquired through the measurements.

1.1 A method to reduce radiation trapping

The methods for reducing radiation trapping that are used today mainly focus on attaining the lifetime for a certain energy level when there are no perturbations. However, when examining the energy levels involved in the Er-Yb laser, this is not the case. The Yb atoms in this laser will not take part in the actual lasing, but acts as a sensitizer, absorbing pump radiation and transferring the absorbed energy to the Er atoms where lasing is achieved. This energy transfer is a non-radiative process, and the efficiency depends both on the proximity of the atoms as well as the lifetimes of the energy levels through which the transfer occurs. However, the depletion of energy levels does not only depend on intrinsic properties in the atoms, but also of the efficiency of the energy transfers in question. The methods for reducing radiation trapping in lifetime measurements most commonly used today will also affect the fluorescence and energy dynamics in the system, and cannot be used in this case, so a new method had to be developed.

Fluorescence that has been reabsorbed and re-emitted seems to originate from a point not overlapped by the pump beam. Using the principles of confocal microscopy, this radiation can be blocked. With the confocal microscopy technique it is possible to look at light originating from one point by placing an aperture in the optically conjugate plane, whereby allowing only for one point to be imaged onto the detector. Hence, off-centre fluorescence will not be detected, which effectively means that light that has been reabsorbed and re-emitted will not reach the detector, and lifetime measurements will be much more accurate. The smaller the aperture in the confocal microscope is, the smaller the area from which fluorescence is detected will be. Ideally, an infinitely small aperture should be used, but naturally this is not implementable. By taking lifetimes measurements at different aperture diameters, the lifetime at zero aperture could be estimated by extrapolating the measurements down to a zero diameter value.

1.2 Simulating radiation trapping

The relation between the measured lifetime and the aperture diameter was not known, and to make accurate predictions based on the measurements taken, further understanding of the processes involved was needed. To gain insight, several numerical simulations were performed, and based on the results from these simulations, the measurements could be understood and properly analyzed. Monte Carlo simulations were also constructed to confirm that the reduction of radiation trapping was the only reason for the shorter lifetimes measured at smaller apertures. By extending the Monte

Carlo simulations, an attempt to simulate the energy transfers in Er-Yb co-doped crystals was made. The results from these simulations were unfortunately inconclusive, most probably due to an incomplete implementation of the physical processes. By assessing these shortcomings, an effective way of calculating these energy transfers could gain a clear insight to the dynamics involved in an Er-Yb laser.

1.3 Outline of the thesis

The disposition of this thesis is as follows: In sections 2, 3 and 4, the basics of laser theory is presented, with an emphasis on quasi-three-level lasers and Er-Yb lasers. In section 5 the theory of non-radiative energy transfers is presented, together with the applications to this thesis. Section 6 will outline the theory of nonlinear optics and describe the OPO used to generate light in the wavelengths needed to perform the lifetime measurements. In section 7, the problems of radiation trapping are presented, as well as a method to reduce them, using a confocal microscope. Also, the results from the measurements as well as the simulations performed to properly understand how to interpret the data can be found there. Section 8 explains the principles of the Monte Carlo simulations, the theory and methods used. The implementation of the Monte Carlo simulation can be found in section 9, as well as an overview of the programs, clarified by a flowchart. The Mote Carlo simulation results are presented in section 10. Finally, a summary of the thesis, together with a discussion of results and methods can be found in section 11, as well as suggestions to future work.

2 Quantisation of energy

In the end of the 19th century physicists were struggling to explain the emission spectrum from a radiating blackbody using a model, Rayleigh-Jean's law, where the energy density per unit frequency would increase with frequency. Not only did it not fit the observed emission spectrum, but it also predicted an infinite amount of energy emitted by the blackbody, (referred to as the ultraviolet catastrophe) which was obviously wrong. To overcome this problem, German physicist Max Planck suggested that electromagnetic radiation could only be emitted in discrete amounts, "quanta". Employing his idea to the blackbody radiator and using Boltzmann's statistical mechanics, it was possible to predict the emission of any blackbody at any temperature, the Planck radiation law [1]:

$$\rho(\nu) = \frac{8\pi h}{c_0} \frac{\nu^3}{e^{\frac{h\nu}{kT}} - 1}, \tag{2.1}$$

where $\rho(\nu)$ is the energy density per unit frequency, h is Planck's constant, ν is the frequency, k is Boltzmann's constant and T is the absolute temperature. At first Planck believed that the quantisation of the emitted energy was just a crude way of solving the problem, however it turned out to be the birth of quantum mechanics. As later shown by Schrödinger (and to some extent Bohr) electrons in atoms can only occupy discrete energy states, and the atom can only absorb or emit energy in agreement with these energy states:

$$E_2 - E_1 = h\nu, \tag{2.2}$$

where E_2 is the final energy state, E_1 is the initial energy state, h is Planck's constant and ν is the frequency of the absorbed or emitted light. In 1917 Albert Einstein proposed that there are three mechanisms in which electromagnetic radiation and atoms interact [2]; (stimulated) absorption, stimulated emission and spontaneous emission. Assuming a two level system of N atoms, where N_1 is in the number of atoms in the ground state and N_2 is the number of atoms in the excited state, Einstein proposed that the rate of stimulated absorption would be proportional to the energy density of the radiation at the specific wavelength of the transition and the number of atoms in the ground state:

$$\frac{dN_1}{dt} = -B_{12}\rho(\nu) N_1, \tag{2.3}$$

and similarly that the rate of stimulated emission would be proportional to the energy density of the radiation and the number of atoms in the excited state:

$$\frac{dN_2}{dt} = -B_{21}\rho(\nu) N_2, \tag{2.4}$$

where B_{12} and B_{21} are proportionality constants with dimension $\left[\frac{m^3}{s^2 J}\right]$. The phase of the stimulated emission would be the same as the external radiation by which it is being stimulated, i.e. the stimulated emission is coherent. Finally he proposed that the rate of spontaneous emission would be proportional to the number of atoms in the upper level:

$$\frac{dN_2}{dt} = -AN_2, \tag{2.5}$$

where A is a proportionality constant with dimension $\left[s^{-1}\right]$. Solving this equation gives

$$N_2 = N_{20} e^{-\frac{t}{\tau}}, \tag{2.6}$$

where $\tau = A^{-1}$ is the life time of the upper level. The phase of the spontaneous emission is random; the photons emitted by this process are incoherent. The rate equations for this two-level system can then be expressed as [3]:

$$\frac{dN_1}{dt} = -\frac{dN_2}{dt} = AN_2 + B_{21}\rho(\nu) N_2 - B_{12}\rho(\nu) N_1. \tag{2.7}$$

In thermal equilibrium the rate equations are equal to zero, there is no net change in the population distribution. Solving for ρ gives:

$$\rho = \frac{AN_2}{B_{12}N_1 - B_{21}N_2} = \frac{A\frac{N_2}{N_1}}{B_{12} - B_{21}\frac{N_2}{N_1}}. \tag{2.8}$$

Using $\frac{N_2}{N_1} = \frac{g_2}{g_1} e^{-\frac{E_2 - E_1}{kT}}$ from statistical physics; where g_1 and g_2 are the degeneracies of level 1 and 2, respectively, the above expression can be simplified to

$$\begin{aligned} \frac{A\frac{N_2}{N_1}}{B_{12} - B_{21}\frac{N_2}{N_1}} &= \frac{A\frac{g_2}{g_1} e^{-\frac{E-E_1}{kT}}}{B_{12} - B_{21}\frac{g_2}{g_1} e^{-\frac{E-E_1}{kT}}} = \\ \frac{A}{B_{12}\frac{g_1}{g_2} e^{\frac{E-E_1}{kT}} - B_{21}} &= \frac{\frac{A}{B_{21}}}{\frac{B_{12}}{B_{21}}\frac{g_1}{g_2} e^{\frac{E-E_1}{kT}} - 1}. \end{aligned} \tag{2.9}$$

Comparing this to the Planck radiation law, Eq.(2.1), the A and B coefficients can be identified:

$$B_{12} = \frac{g_2}{g_1} B_{21}, \tag{2.10}$$

$$A = \frac{8\pi h\nu^3}{c_0} B_{21}. \tag{2.11}$$

These results are valid under the assumption that the external radiation is perfectly matched by the energy separation of the two levels, however

in reality the radiation field is never monochromatic, and this should also be accounted for. The intensity output from an ensemble of exponentially decaying atoms is given by

$$I = I_0 e^{-\gamma t}, \tag{2.12}$$

when I_0 is the intensity at $t = 0$, and $\gamma = 1/\tau$ is the decay rate. By applying a fourier transform to this equation [3], the intensity as a function of frequency is found to be

$$I(\nu) = I_0 \frac{\gamma/4\pi^2}{(\nu - \nu_0)^2 + (\gamma/4\pi)^2}, \tag{2.13}$$

where ν_0 is the centre frequency, and I_0 is defined as $I_0 = \int_0^\infty I(\nu)\, d\nu$. The function

$$S(\nu) = \frac{\gamma/4\pi^2}{(\nu - \nu_0)^2 + (\gamma/4\pi)^2}, \tag{2.14}$$

is called the Lorentzian line-shape function, and describes the broadening mechanism of the emitted radiation. Similarly it can be shown[3] that the

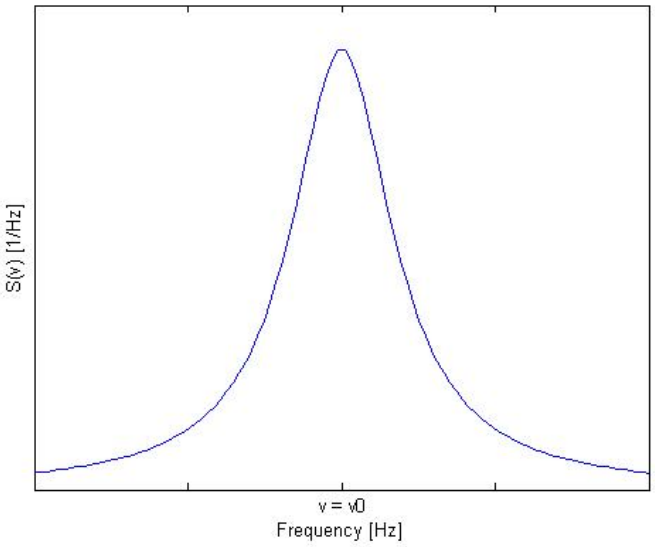

Figure 2.1. *The Lorentzian lineshape.*

Einstein A coefficient is also broadened with a Lorentzian line-shape function, giving a new expression for the Einstein A coefficient:

$$A(\nu) = A \frac{\gamma/4\pi^2}{(\nu - \nu_0)^2 + (\gamma/4\pi)^2}, \tag{2.15}$$

where A is given by $A = \int_0^\infty A(\nu)\, d\nu$. Since the B coefficients are related to the A coefficient, Eq.(2.11), B_{12} and B_{21} are also broadened by the same mechanism, and can now be expressed as:

$$B_{ij}(\nu) = \frac{\gamma/4\pi^2}{(\nu-\nu_0)^2 + (\gamma/4\pi)^2} B_{ij}. \tag{2.16}$$

This type of broadening is called natural or homogeneous broadening, since it occurs for all types of decay in all media, and the broadening is the same for all atoms within a species. There is also inhomogeneous broadenings, e.g. the Doppler broadening which affect gaseous media or broadening mechanisms in glass, where perturbations affect atom lifetimes depending on their position. These types of broadening have a Gaussian line shape, and are generally much larger than the Lorentzian broadening. In this thesis, the only broadening mechanism encountered was homogeneous broadening, since only crystals were used as host material. Crystals are well structured, so all atoms will experience the same perturbations, and since they are placed in a solid, there will be no Doppler broadening.

2.1 Absorption and gain

Now it is possible to model what happens when a beam of intensity I and frequency width $\Delta\nu$ passes through a medium where the atoms have a set of energy levels suitable to absorb and emit the incoming radiation. In this model the spontaneous emission will be neglected, since it does not significantly change the net intensity of the beam. The number of photons absorbed by the atoms per unit volume per unit time is given by [3]:

$$N_1 B_{12}(\nu)\, \Delta\nu \rho(\nu) = N_1 B_{12}(\nu)\, \Delta\nu I(\nu)/c = N_1 B_{12}(\nu)\, I/c, \tag{2.17}$$

where $\rho(\nu) = I(\nu)/c$ has been used. Similarly the stimulated emission per unit volume per unit time can be expressed as:

$$N_2 B_{21}(\nu)\, I/c. \tag{2.18}$$

The energy flux of a surface element dA at position z and $z + dz$ can be described by:

$$[I(z+dz) - I(z)]\, dA = \left[\frac{N_2 B_{21}(\nu)\, I}{c} h\nu - \frac{N_1 B_{12}(\nu)\, I}{c} h\nu\right] dz dA, \tag{2.19}$$

see Fig.(2.2). Simplifying this expression gives:

$$\frac{dI}{dz} = [N_2 B_{21} - N_1 B_{12}] \frac{h\nu}{c}. \tag{2.20}$$

This is a differential equation, and solving it gives:

$$I = I_0 e^{[N_2 B_{21} - N_1 B_{12}] \frac{h\nu}{c} z}. \tag{2.21}$$

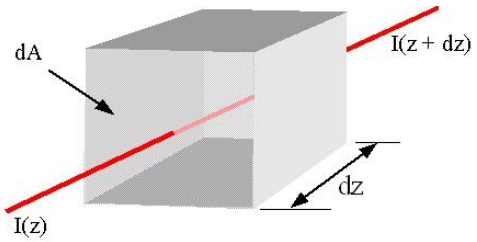

Figure 2.2. *Light with intensity I incident on a medium.*

So, intensity varies exponentially with the distance traveled in the medium. The coefficient in the exponent can be rewritten:

$$\left[N_2 B_{21} - N_1 B_{12}\right] \frac{h\nu}{c} = \left[N_2 - \frac{g_2}{g_1} N_1\right] \frac{c^2}{8\pi\nu^2} A\left(\nu\right) = \Delta N \sigma\left(\nu\right), \tag{2.22}$$

where

$$\Delta N = \left[N_2 - \frac{g_2}{g_1} N_1\right], \tag{2.23}$$

is called the population difference, with dimension $[m^{-3}]$. It compares the population of the upper and lower level, thereby determines whether there will be a net increase or decrease of the beam as it travels in the medium. If more atoms are in the upper level there will be more stimulated emission than absorption, so the beam will increase in intensity with distance traveled. If the opposite is true, there will be more absorption than stimulated emission, and the beam will attenuate.

$$\sigma\left(\nu\right) = \frac{c^2}{8\pi\nu^2} A\left(\nu\right) \tag{2.24}$$

is called the cross section, with dimension $[m^2]$, which describes the atom's "ability" to emit a photon at a specific frequency. Usually the cross section dependence on frequency is understood, and is suppressed, so the intensity of the beam after a distance z in the medium is usually expressed as

$$I = I_0 e^{\sigma \Delta N z}. \tag{2.25}$$

This is sometimes referred to as the Beer-Lambert law.

3 Lasers

By examining Eq.(2.25) one can see it would be possible to amplify a beam if there would be a way of making $\Delta N > 0$ for a specific medium. That is the upper level should be populated by more atoms than the lower level.

3.1 Two-level system

First the two-level system will be examined. In this system there are two energy levels, E_1 which is the ground state of the system, and E_2, the only excited state. If the energy separation between the levels is sufficiently large

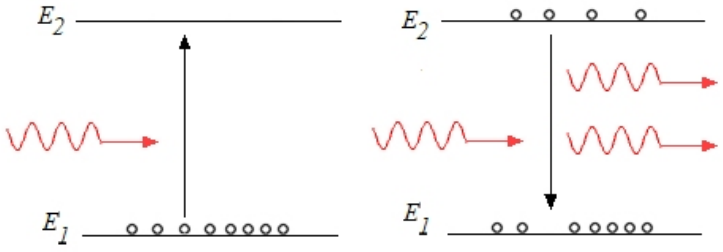

(a) Stimulated absorption *(b) Stimulated emission*

Figure 3.1. *Stimulated emission and absorption in a two-level system.*

there will initially be no population in the excited state, ($\Delta E >> kT$). The only interaction between the atoms and the incident beam will be absorption. As time progresses more atoms will be in the excited state, so the amount of stimulated emission will increase, depopulating the upper level and thus affecting the population difference in a negative way. Still as long as the lower level is more populated absorption will dominate. If the intensity of the beam is increased further, the population difference between the excited and ground state will decrease, until, at very high intensities it will be almost 0, that is $N_2 = N_1$. At this point the stimulated emission and stimulated absorption will be almost equal, since they depend on N_2 and N_1 respectively. At this point half of the photons interacting with the atoms will excite an atom; the other half will stimulate emission. If spontaneous emission is taken in consideration it is obvious that $N_2 = N_1$ is an impossible goal to achieve. There is no way to achieve a positive population difference in a two level system. To further clarify this, the rate equations for the two levels are presented:

$$\frac{dN_1}{dt} = \Gamma N_2 - \Gamma N_1 + \gamma N_2, \tag{3.1}$$

$$\frac{dN_2}{dt} = \Gamma N_1 - \Gamma N_2 - \gamma N_2, \tag{3.2}$$

where Γ is the pump rate and γ is the spontaneous rate of decay. A steady-state solution can be found when $\frac{dN_i}{dt} = 0$, and an expression for the relation between N_1 and N_2 can be determined:

$$\frac{N_2}{N_1} = \frac{\Gamma}{\Gamma + \gamma}. \tag{3.3}$$

As the pump rate Γ is increased sufficiently the spontaneous decay rate γ can be neglected, and hence the ratio approaches unity. However it can never increase beyond unity, thus it is impossible to achieve population inversion in a two-level system.

3.2 Three-level systems

Now a three-level[1] system will be examined. In this case there are three energy levels in the atom that can be accessed, E_1, E_2 and E_3. The incident radiation excites atoms in the ground state, E_1, to the first excited state, E_2. The atom will then rapidly decay from E_2 to E_3. This rapid decay will ensure that there is a minimal stimulated emission from E_2 to E_1 since the atom will only be in E_2 for a very short time. As more and more atoms are transferred from E_1 to E_3 without any detrimental process working in the other direction, since there is virtually no stimulated emission in this process, it could now be possible to have a population inversion, that is a positive population difference, in the levels $E_3 - E_1$. The rate equations for

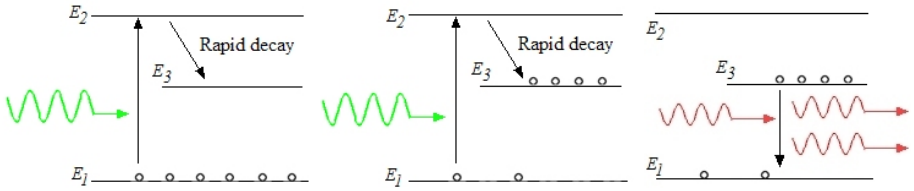

Figure 3.2. *Stimulated emission and absorption in a three-level system.*

this system are:

$$\frac{dN_1}{dt} = \Gamma N_2 - \Gamma N_1 + \gamma_{31} N_3, \tag{3.4}$$

$$\frac{dN_2}{dt} = \Gamma N_1 - \Gamma N_2 - \gamma_{23} N_2, \tag{3.5}$$

$$\frac{dN_3}{dt} = \gamma_{23} N_2 - \gamma_{31} N_3, \tag{3.6}$$

$$\tag{3.7}$$

[1] A system with the ground state energy level as lower laser level is sometimes referred to as a quasi-three-level system. Since the Er and Yb ions are quasi-three-level systems, the theory outlined here will only include the quasi-three-level system.

where Γ is the pump rate, γ_{23} is the spontaneous decay from E_2 to E_3 and γ_{31} is the spontaneous decay from E_3 to E_1. Since there is a rapid decay from E_2 to E_3 the spontaneous decay from E_2 to E_1 will be neglected. Solving these equations for N_3 and N_1, and using the fact that $N_1 + N_2 + N_3 = N$ yields

$$N_1 = \frac{(\Gamma + \gamma_{23})\,\gamma_{31}}{\Gamma\,(\gamma_{23} + \gamma_{31}) + \gamma_{31}\,(\Gamma + \gamma_{23})} N, \tag{3.8}$$

$$N_3 = \frac{\gamma_{23}\Gamma}{\Gamma\,(\gamma_{23} + \gamma_{31}) + \gamma_{31}\,(\Gamma + \gamma_{23})} N. \tag{3.9}$$

To check if population inversion is possible to achieve between the E_3 and E_1 states, the ratio N_3/N_1 will be examined:

$$\frac{N_3}{N_1} = \frac{\gamma_{23}\Gamma}{(\Gamma + \gamma_{23})\,\gamma_{31}}. \tag{3.10}$$

The ratio should be greater than 1 for population inversion of the system. To calculate the pump rate necessary for population inversion Γ is solved for:

$$\frac{\gamma_{23}\Gamma}{(\Gamma + \gamma_{23})\,\gamma_{31}} > 1 \Rightarrow \Gamma > \frac{\gamma_{31}}{1 - \frac{\gamma_{31}}{\gamma_{23}}} \approx \gamma_{31}. \tag{3.11}$$

As mentioned previously, the spontaneous rate γ_{23} is fast, so the quotient γ_{32}/γ_{23} is small. Neglecting that term gives a simpler expression which says that the pump rate has to be higher than the spontaneous decay rate from E_3 to E_1 in order to achieve population inversion of the system.

3.3 Four-level system

Lastly a 4 level system will be examined. There are now four energy levels that can be accessed by external radiation, E_1, E_2, E_3 and E_4. The external

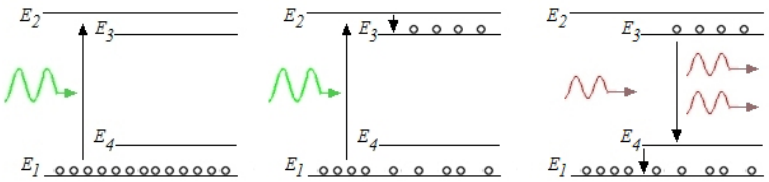

Figure 3.3. *Stimulated emission and absorption in a four-level system.*

radiation pumps atoms from the ground state E_1 to E_2. As in the three-level system, the decay from E_2 to E_3 can be very fast, so there will be an almost immediate depletion of the level E_2. If the transition E_3 to E_4 is slow, there will be a build-up of atoms in E_3. Also, if the transition E_4 to E_1 is very rapid, the population difference could be very large. Fulfilling

these requirements give a very easy way of achieving population inversion. The rate equations of the system are:

$$\frac{dN_1}{dt} = \Gamma N_2 - \Gamma N_1 + \gamma_{41} N_4, \tag{3.12}$$

$$\frac{dN_2}{dt} = \Gamma N_1 - \Gamma N_2 - \gamma_{23} N_2, \tag{3.13}$$

$$\frac{dN_3}{dt} = \gamma_{23} N_2 - \gamma_{34} N_3, \tag{3.14}$$

$$\frac{dN_4}{dt} = \gamma_{34} N_3 - \gamma_{41} N_4. \tag{3.15}$$

Again it is possible to find the ratio of the two interesting energy levels, E_3 and E_4:

$$\frac{N_3}{N_4} = \frac{\gamma_{41}}{\gamma_{34}}. \tag{3.16}$$

If a system has a very high rate of decay from E_2 and E_4, and a much slower rate of decay from E_3 to E_4, this ratio can be very high. This effectively means that all photons pumped from the ground state ends up in the upper laser level, and the lower laser level is virtually empty, so population inversion can be achieved from pump photon number one. In a three-level system, many atoms have to be pumped to the upper laser level just to depopulate the lower laser level. Comparison of the pump rates necessary for population inversion in the 3 and four-level system can be seen in Fig.(3.4) [4].

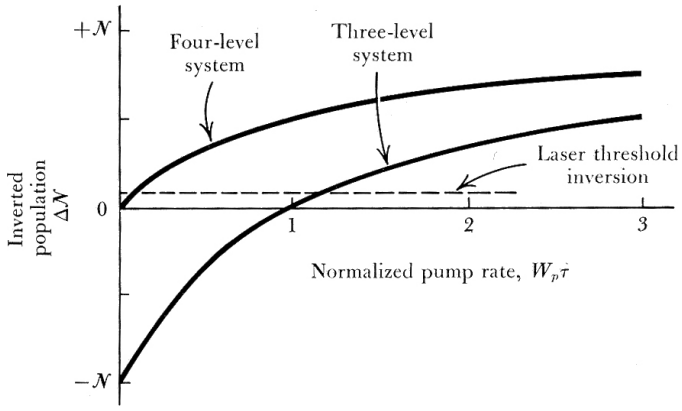

Figure 3.4. *A schematic showing the differences in pumping to achieve population inversion in three-level and four-level systems.*

As seen in the figure, much less pumping is needed in a four-level system to achieve population inversion than in a three-level system.

4 Tree-level Er and Yb-Er lasers

In this section a three-level system consisting of an Er^{3+}-doped and an Er^{3+} - Yb^{3+}-co-doped solid-state laser will be considered. Er is a member of the lanthanide group in the periodic system. Generally, rare-earth elements have a suitable laser transition in the inner shells, which are shielded from the surrounding host material. This limits quenching and thus a stable long-lived upper laser level can be found in numerous rare earths. The energy level diagram for Er is presented in Fig.(4.1) where the dashed lines represent

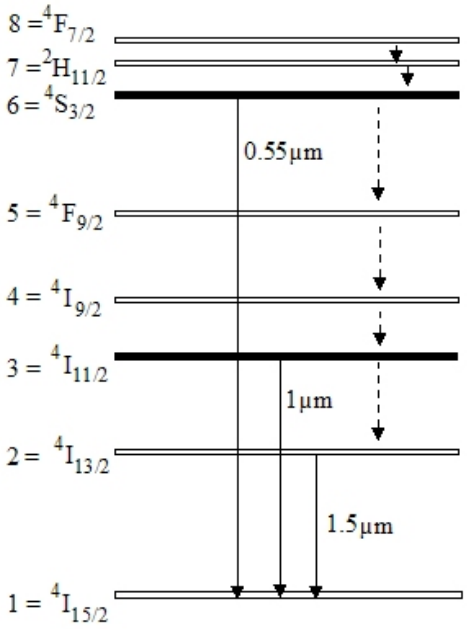

Figure 4.1. *Energy level diagram of the Er system.*

non-radiative transitions. This is a three-level system, and can be pumped to the $^4S_{3/2}$ level and then use $^4I_{11/2}$ as the upper laser level. However there is a quite large energy difference between the pump level and the upper laser level, which means that a large portion of the pump energy will be converted into heat. This energy difference is referred to as the quantum defect, and sets the limit on the power efficiency of the laser. If there are no other losses in the system, the maximum power efficiency would be the ratio of laser to pump photon energy. The remaining energy is absorbed by the host material through phonon transitions or emitted as fluorescence. If the host material in which Er^{3+} is doped is sensitive to heat this could effectively limit the pump power used, and hence the output power of the laser. This is the case for many Er^{3+} glass lasers, for which the maximum average output power is limited due to the poor thermal conductivity of the

glass host.

It is also possible to pump the system at 980 nm to the $^4I_{11/2}$ level. The absorption cross section for Er^{3+} at this wavelength is unfortunately quite poor, so to counter this, a much higher doping concentration is needed. As the $^4I_{15/2}$ is both the ground state level and the lower laser level, increasing the doping concentration will also have the detrimental effect of raising the laser threshold pump power, again needing a higher pump power which also generates more heat to the surrounding host material.

4.1 Er-Yb system

One way to circumvent this problem is to add a sensitizer ion, which has a significantly higher cross section at the desired pump wave length. The excited sensitizer ion can then transfer its energy to an Er^{3+} ion, increasing the pumping efficiency. For this purpose the Yb^{3+} ion is often used:

$$Er^{3+} + {}^*Yb^{3+} \rightarrow {}^*Er^{3+} + Yb^{3+}, \tag{4.1}$$

where the asterisk represents an ion in the excited state. Fig. 4.2 shows the

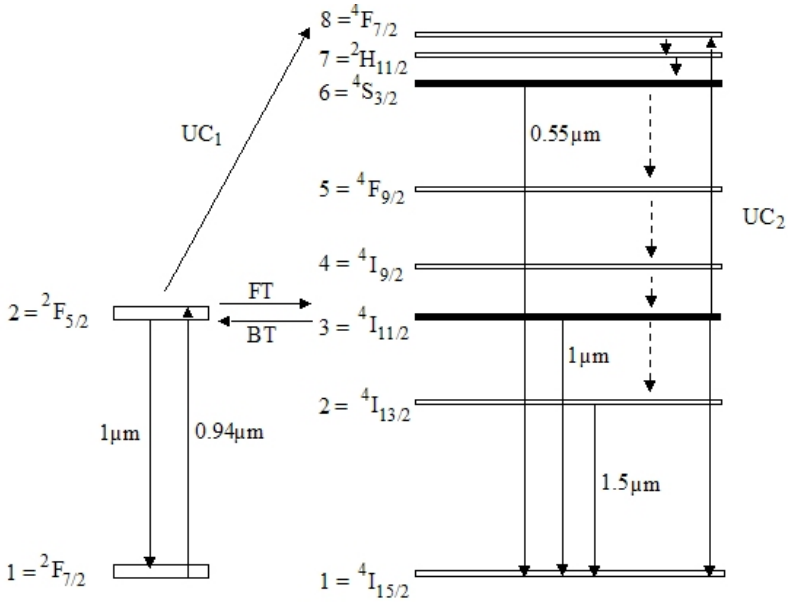

Figure 4.2. *Energy level diagram of the Er-Yb system.*

energy level diagram for the Er^{3+} - Yb^{3+} system. *FT* is short for forward transfer, the process in which an Yb^{3+} ion transfers its energy to a nearby Er^{3+} ion. *BT*, back transfer, is the reverse process, in which an excited Er^{3+} ion transfers its energy to a neighbouring Yb^{3+} ion. Upconversion (*UC*) is a process in which two excited ions interact and exchange energy. There

are two main types of upconversion processes, although more upconversions have been suggested, [5]; the cumulative upconversion, UC_1, and the cooperative upconversion, UC_2. In the cumulative process one Yb^{3+} transfers its excitation energy to an Er^{3+} ion in the $^4I_{11/2}$ state, resulting in an Er^{3+} in the $^4F_{7/2}$ state and an Yb^{3+} in the ground state. In the cooperative upconversion process two Er^{3+} ions in the $^4I_{11/2}$ redistributes the excitation energy so that one falls down to the ground state and one is bumped up to the $^4F_{7/2}$. Of course the reverse processes are also theoretically possible; however the $^4F_{7/2}$ state is very short-lived, so the probability for an upconversion process occurring "backwards" is very small. The upconversion processes are detrimental to the laser, since one pump photon is wasted for every upconversion event.

4.1.1 Rate equation analysis of the Er-Yb system

The following section will outline the theory presented in the Doctoral thesis "Diode pumped rare-earth-doped quasi-three-level laser" by Stefan Bjurshagen.

To properly investigate the dynamics in the Er-Yb system the rate equations for the relevant levels are presented:

$$\begin{aligned}
\frac{dN_{Yb,2}}{dt} &= \Gamma N_{Yb,1} - \frac{N_{Yb,2}}{\tau_{Yb}} - k_{FT}N_{Yb,2}N_{Er,1} - k_{UC,1}N_{Yb,2}N_{Er,3} \quad (4.2)\\
&\quad + k_{BT}N_{Yb,1}N_{Er,3},\\
\frac{dN_{Er,6}}{dt} &= \gamma_{nr,6}N_{Er,6} - \frac{N_{Er,6}}{\tau_{Er,6}} + k_{UC,1}N_{Yb,2}N_{Er,3} - k_{UC,2}N_{Er,6}^2, \quad (4.3)\\
\frac{dN_{Er,3}}{dt} &= -\gamma_{nr,3}N_{Er,3} - \frac{N_{Er,3}}{\tau_{Er,3}} - k_{BT}N_{Yb,1}N_{Er,3} \quad (4.4)\\
&\quad + k_{FT}N_{Yb,2}N_{Er,1} - k_{UC,1}N_{Yb,2}N_{Er,3} - 2k_{UC,2}N_{Er,6}^2\\
&\quad + \gamma_{nr,6}N_{Er,6} + \beta_{63}\frac{N_{Er,6}}{\tau_{Er,6}},\\
\frac{dN_{Er,2}}{dt} &= -\frac{N_{Er,2}}{\tau_{Er,2}} + \gamma_{nr,3}N_{Er,3} + \beta_{32}, \frac{N_{Er,3}}{\tau_{Er,3}} + \beta_{62}\frac{N_{Er,6}}{\tau_{Er,6}}, \quad (4.5)\\
N_{Yb} &= N_{Yb,1} + N_{Yb,2}, \quad (4.6)\\
N_{Er} &= N_{Er,1} + N_{Er,2} + N_{Er,3} + N_{Er,6}, \quad (4.7)
\end{aligned}$$

where N_{Yb1-2} and N_{Er1-6} are the energy levels of Yb and Er shown in Fig.(4.2). Γ is the pump rate; k_{FT} and k_{BT} are the forward and back transfer coefficient respectively. τ_{Yb} and $\tau_{Er,2-6}$ are the radiative lifetimes from the indicated levels, $\gamma_{nr,3}$ and $\gamma_{nr,3}$ are the non-radiative lifetimes from levels $Er,3$ and $Er,6$ respectively. $k_{UC,1}$ and $k_{UC,2}$ are the upconversion coefficients, and β_{ij} is the branching ratio from level i to level j, i.e. the probability that an atom spontaneously decaying from level i ends up in

level j. N_{Er} and N_{Yb} are the total doping concentrations in the material. In order to investigate the forward transfer and back transfer processes under rapid, short pulsed excitation, some approximations can be made. At low excitations the population in the ground state will be almost unaffected, allowing the transfer rates $W_{FT} = k_{FT}N_{Er}$ and $W_{BT} = k_{BT}N_{Yb}$ to be used. Further, the upconversion processes are relatively weak, and are therefore ignored, as is the radiative decay from $Er, 3$, since the non-radiative decay is much faster. The rate equations for $N_{Yb,2}$ and $N_{Er,3}$ can now be expressed as:

$$\frac{dN_{Yb,2}}{dt} = W_{BT}N_{Er,3} - \left(\frac{1}{\tau_{Yb}} + W_{FT}\right) N_{Yb,2}, \tag{4.8}$$

$$\frac{dNEr,3}{dt} = W_{FT}N_{Yb,2} - \left(\gamma_{nr,3} + W_{BT}\right) N_{Er,3}. \tag{4.9}$$

This is a linear system which can be solved for $N_{Yb,2}$ and $N_{Er,3}$:

$$N_{Yb,2}(t) = C_{11}e^{-W_{eff,1}t} + C_{12}e^{-W_{eff,2}t}, \tag{4.10}$$

$$N_{Er,3}(t) = C_{21}e^{-W_{eff,1}t} + C_{22}e^{-W_{eff,2}t}, \tag{4.11}$$

where $W_{eff,1}$ and $W_{eff,2}$ are

$$W_{eff,1} = \frac{W_{FT} + W_{BT} + 1/\tau_{Yb} + \gamma_{nr,3}}{2} + \frac{1}{2}\sqrt{\left(W_{FT} - W_{BT} + 1/\tau_{Yb} - \gamma_{nr,3}\right)^2 + 4W_{FT}W_{BT}}, \tag{4.12}$$

$$W_{eff,2} = \frac{W_{FT} + W_{BT} + 1/\tau_{Yb} + \gamma_{nr,3}}{2} - \frac{1}{2}\sqrt{\left(W_{FT} - W_{BT} + 1/\tau_{Yb} - \gamma_{nr,3}\right)^2 + 4W_{FT}W_{BT}}, \tag{4.13}$$

and the constants C_{ij} are given by the initial conditions at $t = 0$:

$$C_{11} = N_{Yb,2}(0)\frac{W_{FT} + 1/\tau_{Yb} - W_{eff,2}}{W_{eff,1} - W_{eff,2}}, \tag{4.14}$$

$$C_{12} = N_{Yb,2}(0) - C_{11}, \tag{4.15}$$

$$C_{21} = C_{11}\frac{W_{FT} + 1/\tau_{Yb} - W_{eff,1}}{W_{BT}}, \tag{4.16}$$

$$C_{22} = -C_{21}. \tag{4.17}$$

$W_{eff,1}$ can be interpreted as both the effective decay rate for $Yb, 2$ and the effective rise rate for $Er, 3$ at the initial time. At later times the slower effective decay rate $W_{eff,2}$ dominates,which leads to an equal single exponential decay from $Yb, 2$ and $Er, 3$, see Fig.(4.3). If $1/\tau_{Yb}$ and $\gamma_{nr,3}$ are of the same order, a Taylor expansion around $1/\tau_{Yb} = \gamma_{nr,3}$ for $W_{eff,2}$ yields

$$W_{eff,2} \approx 1/\tau_{Yb} + \frac{\gamma_{nr,3} - 1/\tau_{Yb}}{1 + \left(W_{FT}/W_{BT}\right)^{-1}}. \tag{4.18}$$

Apparently, the effective decay rate is dependent of the ratio W_{FT}/W_{BT}, and thus also the $[Er3+]/[Yb3+]$ concentration.

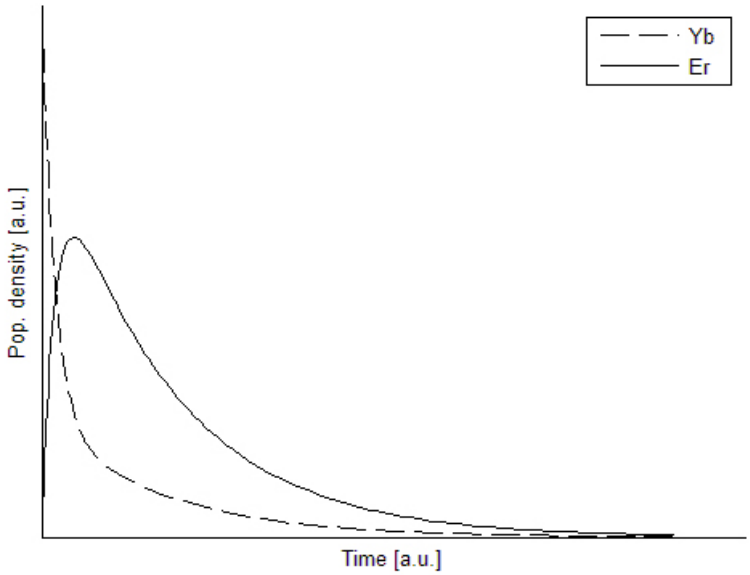

Figure 4.3. *Rate dynamics of the Er-Yb system.*

5 Non-radiative energy transfer

As seen in previous chapters, there are a number of different processes in which closely positioned atoms exchange energy; the forward and back transfer processes as well as upconversion are examples of these. In this chapter these processes will be examined and a theory to explain these processes will be presented.

In the simplest approximation the interaction between atoms and light can be considered as a dipole interaction between the electric field and the atomic dipole moment, the so-called dipole approximation. In quantum mechanics, the probability of a transition from an initial state Ψ_i to a final state Ψ_f is given by

$$P = \left\langle \Psi_f \left| \hat{H}_{ed} \right| \Psi_i \right\rangle, \tag{5.1}$$

where $\hat{H}_{ed}$ is the electric dipole Hamiltonian, $\hat{H}_{ed} = -e\sum_i \hat{r}_i$, simply the dipole moment between the final and initial state. If now considering two atoms so close to each other that the atomic dipole moments can interact directly with each other there will be a possibility of a direct, non-radiative transfer of energy from one atom to the other. This interaction was first considered by the German chemist Theodore Förster. He showed that the rate in which a set of donor atoms transfers energy to a set of acceptor atoms is proportional to the absolute square of the interaction Hamiltonian, in this case a dipole-dipole interaction Hamiltonian:

$$W_{DA} \propto \left| \hat{H}_{dip-dip} \right|^2, \tag{5.2}$$

where the dipole-dipole interaction Hamiltonian is given by the expression

$$\hat{H}_{dip-dip} = \frac{1}{4\pi\varepsilon_0} \left[(\hat{\mu}_D \cdot \hat{\mu}_A - 3\,(\hat{\mu}_D \cdot \hat{r})\,(\hat{\mu}_A \cdot \hat{r})) \right] \frac{1}{R^3}, \tag{5.3}$$

where R is the distance between the dipoles, $\hat{r}$ is the unit vector, $\hat{\mu}_D$ is the donor dipole moment and $\hat{\mu}_A$ is the acceptor dipole moment, see Fig.(5.1).

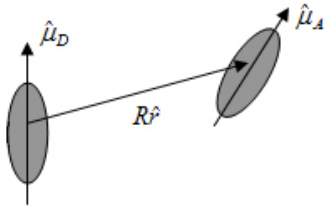

Figure 5.1. *A schematic of the dipole-dipole interaction.*

Generally, the donor atom and the acceptor atom are of different species, however there is also a possibility for a donor atom to transfer its energy

to an atom of the same species, i.e. donor-donor interactions. This process is usually referred to as energy migration in the case of the acceptor atom being of the same species as the donor atom (D-D interactions), and energy transfer if they are different (D-A interactions). The rate for these processes can be shown to be [6]:

$$W_{DX} = \frac{1}{\tau_{rad}} \left(\frac{R_{DX}}{r} \right)^6, \tag{5.4}$$

where X can be either an acceptor, A, or another donor, D. τ_{rad} is the radiative life time of the donor in absence of this process, and R_{DX} is the Förster radius, the distance in which the rate of energy transfer by dipole-dipole coupling equals the fluorescence decay rate. This can be calculated through the cross section overlap function [6]:

$$R_{DX}^6 = \frac{3c\tau_{rad}}{8\pi^4 n^2} \int \sigma_D^{em}(\lambda) \sigma_X^{abs}(\lambda)\, d\lambda, \tag{5.5}$$

where c is the speed of light, n is the refractive index in the material, $\sigma_D^{em}(\lambda)$ is the emission cross section of the donor atom and $\sigma_X^{abs}(\lambda)$ is the absorption cross section of the donor or acceptor atom. The total rate of decay from the donor ensemble in the excited state in absence of other processes is

$$W_{tot} = W_{rad} + W_{DA} = \frac{1}{\tau_{rad}} + \frac{1}{\tau_{rad}} \sum_i \sum_j \left(\frac{R_{DA}}{r_{ij}} \right)^6, \tag{5.6}$$

where r_{ij} is the distance from the donor i to acceptor j. Assuming a system of only one donor, Eq.(5.6) simplifies to

$$W_{tot} = \frac{1}{\tau_{rad}} + \frac{1}{\tau_{rad}} \sum_i \left(\frac{R_{DA}}{r_i} \right)^6. \tag{5.7}$$

To investigate the probability of the donor atom relaxing through energy transfer the ratio W_{DA}/W_{tot} is taken:

$$P = \frac{\sum_i \left(\frac{R_{DA}}{r_i} \right)^6}{1 + \sum_i \left(\frac{R_{DA}}{r_i} \right)^6}. \tag{5.8}$$

As seen this is independent of the fluorescence life time, it varies only with the distance between interacting atoms and the Förster radius. Since this interaction decreases with r^{-6} it will have practically no significance if the average distance between neighbouring atoms is more than two Förster radii, as can be seen in Fig (5.2).

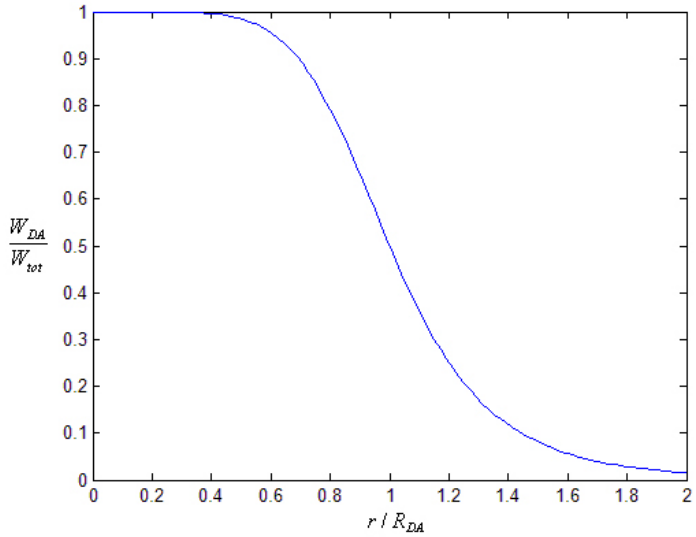

Figure 5.2. *The graph shows how probable the energy transfer is, depending on the distance to a neighbouring atom.*

5.1 McCumber theory

Measuring the emission cross section σ_D^{em} needed in Eq.(5.5) can be quite difficult when the absorption and emission wavelengths are very close. However under certain conditions it is possible to calculate the emission cross section from the absorption cross section [7, 8]. Consider Fig.(5.3) which shows an energy level diagram for two Stark level manifolds. The individual Stark levels of the upper manifold are labeled i and the Stark levels of the lower manifold are labeled j. The energy difference between the lowest Stark level of the upper manifold and the lowest Stark level of the lower manifold is labeled E_0, the energy difference between the Stark level i and the lowest level in the upper manifold is labeled Δ_i, and the energy difference between the Stark level j and the lowest level in the lower manifold is labeled Δ_j. The individual Stark levels are assumed to be thermally populated. Each transition between two Stark levels are connected with a cross section $\sigma_{ij}(\nu) = \sigma_{0ij} g_{ij}(\nu - E_{ij}/h)$ where $g_{ij}(\nu)$ is related to the Lorentzian line shape function, normalized so that $g_{ij}(0) = 1$, and σ_{0ij} is the peak cross section at $\nu = E_{ij}/h$. By summing the cross sections of all transitions from the upper to the lower manifold and weighting them by their thermal population distribution, an expression for the total emission cross section from the upper to the lower manifold can be determined:

$$\sigma_{em}(\nu) = \sum_i \sum_j \frac{\sigma_{ij}(\nu)\, e^{-\beta \Delta i}}{Z_{up}}, \tag{5.9}$$

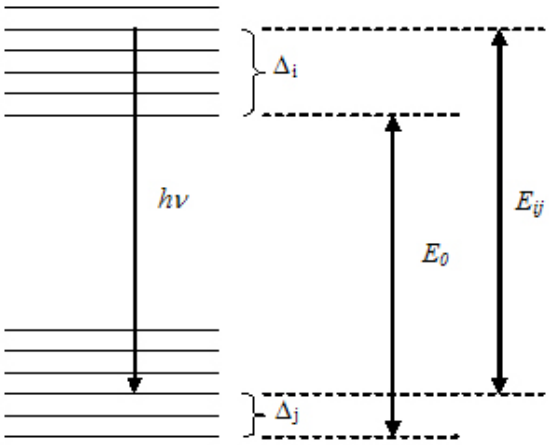

Figure 5.3. *Two Stark level manifolds and their defined transition energies.*

where Z_{up} is the partition function of the upper manifold and $\beta = (kT)^{-1}$. With the same reasoning the absorption cross section can be written

$$\sigma_{abs}(\nu) = \sum_j \sum_i \frac{\sigma_{ji}(\nu) e^{-\beta \Delta j}}{Z_{low}}, \tag{5.10}$$

where Z_{low} is the partition function of the lower manifold. Note from Fig.(5.3) that Δ_i can be expressed in terms of the other defined energy differences:

$$\Delta_i = \Delta_j + E_{ij} - E_0. \tag{5.11}$$

Inserting this in Eq.(5.9) gives:

$$\begin{aligned} \sigma_{em}(\nu) &= \sum_i \sum_j \frac{\sigma_{ij}(\nu) e^{-\beta(\Delta j + E_{ij} - E_0)}}{Z_{up}} \\ &= \sum_i \sum_j \frac{\sigma_{ij}(\nu) e^{-\beta \Delta j} e^{-\beta(E_{ij} - h\nu)} e^{\beta(E_0 - h\nu)}}{Z_{up}}. \end{aligned} \tag{5.12}$$

The exponent in the middle term in the last expression in Eq.(5.12), $\beta(E_{ij} - h\nu)$, can be neglected under the condition that the energy width of each individual Stark level is small compared to kT, i.e.

$$\beta |E_{ij} - h\nu| \ll 1, \tag{5.13}$$

which means that Eq.(5.12) simplifies to

$$\sigma_{em}(\nu) \cong \frac{1}{Z_{up}} \left[\sum_i \sum_j \sigma_{ij}(\nu) e^{-\beta \Delta j} \right] e^{\beta(E_0 - h\nu)} = \frac{Z_{low}}{Z_{up}} \sigma_{abs}(\nu) e^{\beta(E_0 - h\nu)}, \tag{5.14}$$

where in the last step $\sigma_{ij} = \sigma_{ji}$ is used, so the expression in the brackets can be identified as the absorption cross section multiplied by the lower manifold partition function. Thus under the assumptions that the energy of the individual Stark levels are small compared to kT and that the manifolds are thermally populated, the absorption cross section can be calculated from the emission cross section by:

$$\sigma_{em} \cong \frac{Z_{low}}{Z_{up}} \sigma(\nu)_{abs} e^{\beta(E_0 - h\nu)}. \tag{5.15}$$

5.2 Application

When doing calculations on the energy transfer efficiency, it is very important to know the Förster radius as accurately as possible. Note that the Förster radius is not connected to one atom species, but is related to both the donor and acceptor atom cross sections. This means that in order to accurately simulate the energy transfer and migration, four radii has to be calculated, R_{DD}, R_{DA}, R_{AD} and R_{AA}. Also this means that R_{DA} and R_{AD} will not necessarily be the same. For the system studied in the thesis, the Yb atoms are the donors, since only they are being pumped, and hence the Er atoms are the acceptors. To calculate the radii needed, the absorption cross sections of Er and Yb doped in KLuW were acquired [2], see Fig.(5.4). Note that the Er atoms have almost one order of magnitude smaller cross section than Yb, which is why Yb atoms are used as sensitizer ions. The cross sections provided to us were actually three cross sections per crystal, one for each of the optical axes; p, n, and g, in the crystal. In the simulations described in section 8, the polarisation of the fluorescence is assumed to be random and isotropic, so an average of the three cross sections are taken, for simplicity. The emission cross sections of Er and Yb are calculated with Eq.(5.15), and the result can be seen in Fig.(5.5).

A curios detail that can be seen in the Er emission spectrum is the behaviour at the longer wavelengths, where the cross section goes up, it looks a bit like amplified noise. This is in fact precisely what it is. When deriving the McCumber relation, Eq.(5.15), the assumption in Eq.(5.13) had to be made. If this assumption does not hold, every term will be multiplied by a factor $e^{\beta(E_{ij} - h\nu)}$, which means that everything to the right of the peak in Fig.(5.5) will be exponentially growing with wavelength, and everything to

[2] Thank you M. C. Pujol, Universitat Rovira i Virgili, Tarragona, Spain

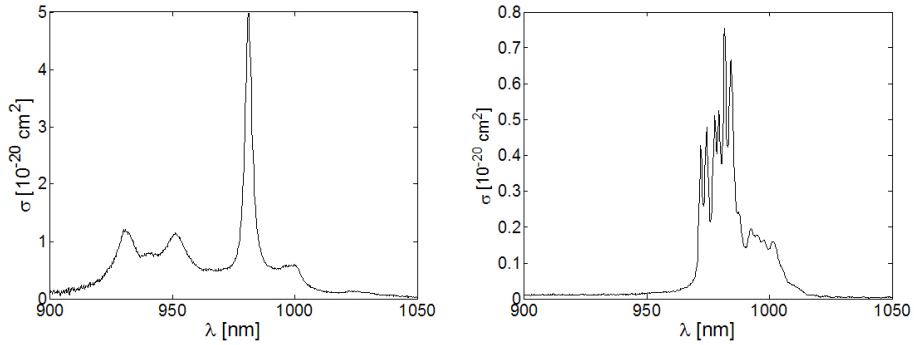

(a) The average Yb absorption cross section. *(b) The average Er absorption cross section.*

Figure 5.4. *The average absorption cross section of Yb and Er atoms in KLuW.*

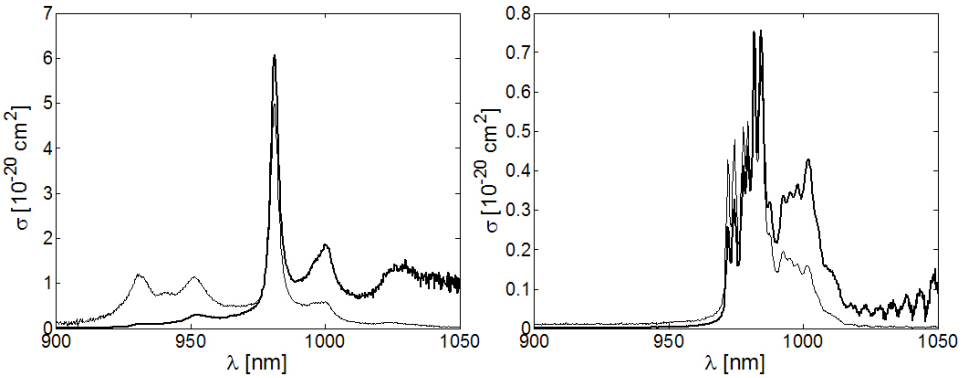

Figure 5.5. *The graphs show the emission cross section, bold lines, and absorption cross section, thin lines, for Yb, to the left, and Er, to the right.*

the left of the peak will decay with wavelength [8]. This will cause some problems, since a distorted emission cross section will cause bad values when the Förster radii are calculated. To completely overcome this problem, measured values should be used for the emission and absorption cross section, alternatively, another way of calculating the emission cross section from the absorption cross section should be used.

However, ignoring this error in the emission cross section, the Förster radii can be calculated, using Eq.(5.5) and Eq.(5.15):

$$R_{YbEr} = 10.95\text{Å},$$
$$R_{YbYb} = 14.63\text{Å},$$
$$R_{ErYb} = 15.36\text{Å},$$
$$R_{ErEr} = 12.19\text{Å}.$$

The shortest interaction length seems to be the Yb-Er interaction, which is not so good, since that is the interaction of most interest. There are however other factors that determine the efficiency of the transfers, not just the interaction lengths. A large amount of non-radiative decay, for example, will reduce the rate of non-radiative energy transfers, something seen in the Er system with phonon transitions between $^4\mathrm{I}_{11/2}$ and $^4\mathrm{I}_{13/2}$, see Fig.(4.2).

6 Nonlinear optics

In this section the basic principles of nonlinear optics will be presented, along with the applications to this thesis.

6.1 Basic theory of nonlinear optics

When an electromagnetic wave propagates through a dielectric medium it will induce a polarisation in the medium. For most situations and media, this can be described by [9]:

$$P = \varepsilon_0 \chi E, \tag{6.1}$$

where E is the electric field, ε_0 is the electric permittivity, χ is the susceptibility of the medium and P is the polarisation, i.e. the induced dipole moment. However, if the electric field is sufficiently strong, the relation between E and P is no longer linear, so P can be expressed as a power series in E [9]:

$$P = \varepsilon_0 \left(\chi^{(1)} E + \chi^{(2)} E^2 + \chi^{(3)} E^3 + \cdots \right). \tag{6.2}$$

The terms $\chi^{(2)}$ and $\chi^{(3)}$ are known as the second and third order nonlinear susceptibilities, respectively. Assuming there are no free charges in the medium, and that the electromagnetic wave is an infinite plane wave, the wave equation in this dielectric medium has the form:

$$\nabla^2 E - \frac{1}{c^2} \frac{\partial^2 E}{\partial t^2} = \mu_0 \frac{\partial^2 P}{\partial t^2}, \tag{6.3}$$

where μ_0 is the permeability of free space and c is the speed of light in vacuum. If Eq.(6.1) is substituted into Eq.(6.3) and using $c = (\varepsilon_0 \mu_0)^{-\frac{1}{2}}$ the result is the wave equation in a linear optical medium:

$$\nabla^2 E - \frac{1 + \chi}{c^2} \frac{\partial^2 E}{\partial t^2} = 0, \tag{6.4}$$

where $1 + \chi$ can be identified as the squared refractive index of the medium. However, if higher order terms of the electric field are considered the results will not be so simple. In this thesis only second order effects have been used, so only the theory for second order nonlinear optics will be presented, which means that the first and second order terms in Eq.(6.2) are considered, and higher order terms are ignored. Assuming that the incident light in the medium is an infinite plane wave, the electric field takes the form $E(\mathbf{r}, t) = \left(E_0 e^{i(\omega t - \mathbf{k} \cdot \mathbf{r})} + c.c. \right)$, where *c.c.* is short for the complex conjugate. Using this in Eq.(6.3), together with the new expression for P:

$$P = \varepsilon_0 \left(\chi^{(1)} E + \chi^{(2)} E^2 \right), \tag{6.5}$$

and solving for P result in three terms. One term is just the linear polarisation, but the other terms are new:

$$P(\mathbf{r},t) = 2\chi^{(2)}E_0E_0^* + \chi^{(2)}\left(E_0^2e^{i(2\omega t - 2\mathbf{k}\cdot\mathbf{r})} + c.c.\right), \tag{6.6}$$

where E_0^* is the complex conjugate of E_0. The first term in Eq.(6.6) describes a phenomenon known as light rectification; there will be a static field created by the polarisation. The expression in the brackets describes a phenomenon in which the polarisation oscillates with the angular frequency 2ω. This oscillation will, according to Larmor's theorem, generate an electromagnetic field with the same frequency, thus light with twice the angular frequency of the incident light will be generated. This process is known as second-harmonic generation. Without losing generality the problem can be simplified to one dimension by letting $\partial/\partial x = \partial/\partial y = 0$, and solving Eq.(6.3) for E in the case of a monochromatic field will yield a set of coupled wave equations:

$$\frac{\partial E_{01}}{\partial z} = \frac{i\omega_1}{n_1c}\chi^{(2)}E_{03}E_{02}^*e^{-i\Delta kz}, \tag{6.7}$$

$$\frac{\partial E_{02}}{\partial z} = \frac{i\omega_2}{n_2c}\chi^{(2)}E_{03}E_{01}^*e^{-i\Delta kz}, \tag{6.8}$$

$$\frac{\partial E_{03}}{\partial z} = \frac{i\omega_3}{n_3c}\chi^{(2)}E_{01}E_{02}e^{i\Delta kz}, \tag{6.9}$$

where E_{0i} is the amplitude of the i:th wave, n_i is the refractive index experienced by wave i and $\Delta k = k_1 + k_2 - k_3$ is the phase mismatch, the momentum difference between the different waves. This is a three-photon process, and depending on the phase matching condition, different processes can be observed in a general non linear material, see Fig.(6.1)

Figure 6.1. *Two general non-linear processes; two incoming waves mixing, resulting in SHG, SFG, and DFG; or energy from one wave dividing between two generated output waves resulting in OPO and OPG.*

These processes can be divided into two categories, one in which two incoming waves interact to generate a third wave with a frequency of the sum

or difference of the incoming waves; $\omega_3 = \omega_1 \pm \omega_2$. These processes are known as sum frequency generation, SFG, and difference frequency generation, DFG. A special case of SFG is where $\omega_1 = \omega_2, \omega_3 = 2\omega_1$, which is known as second harmonic generation, SHG, also described above. The second category is where one incoming wave generates two waves with frequencies $\omega_1 + \omega_2 = \omega_3$. This process is known as optical parametric generation, OPG, or optical parametric oscillation, OPO, depending on the nature of the set-up. In this thesis an OPO has been used extensively in experimental set-ups, and will be described in more detail below.

6.2 Optical parametric oscillator

The process of optical parametric generation can be described as the process in which energy from an incoming beam, the pump, is distributed between two new beams, the signal and the idler, in a nonlinear process. If looking at this process in a photon perspective, the energy of one pump photon is divided into two photons. Energy conservation then states that $\omega_{pump} = \omega_{signal} + \omega_{idler}$. It is common to name the higher of the two frequencies signal and the lower idler. To improve the efficiency of this process one can place the set-up in a resonator. This set-up is referred to as an OPO, an optical parametric oscillator. In the most common set-up, the cavity is set up in such a way that the signal or idler is resonated, see Fig.(6.2)

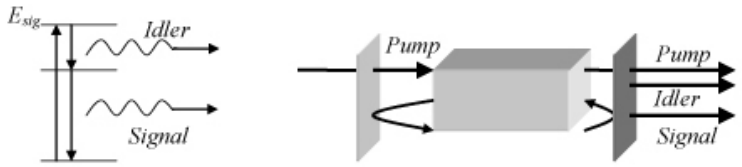

Figure 6.2. *The energy diagram representing an OPO, together with a schematic of the set-up.*

The OPO can be very useful when specific wavelengths are needed, and other laser sources are incapable of producing them. It is also tunable, which means that any wavelength within a certain interval can be generated. Depending on the application of the output, either the signal or idler can be resonated. By resonating the signal, a better beam quality is achieved, but also a lower power output. If the output power is more important the idler could be resonated, however the beam quality of the signal is then worse.

7 Accurate lifetime measurements in tungstate crystals

Knowing the lifetimes of the energy levels involved in a laser is imperative when designing a laser system. Different host materials affect the lifetimes of the energy levels, so choosing a host material is not just about choosing the material with the highest thermal conductivity or the highest thermal damage threshold, one also has to consider how the dopant behaves in the host material. For example, the ${}^4I_{11/2}$ level in Er^{3+}, see Fig.(4.2), has a lifetime of around 2 μs in glass but in the crystal KGW it has a lifetime of around 150 μs, making back transfer from Er to Yb much more likely. To properly know the different lifetimes, multiple set-ups were made to measure relevant lifetimes in different crystals and doping concentrations.

7.1 Avoiding radiation trapping

When taking measurements it is important to try and eliminate and minimize as many sources of errors as possible. The process that seriously affects the result in these measurements is radiation trapping, i.e. reabsorption and re-emission of fluorescence within the crystal. The fluorescence gets "trapped" inside the crystal, it does not exit the crystal right away, but is absorbed by another dopant before it reaches the crystal surface. This means that when a fluorescence photon finally leaves the crystal, it is delayed by the reabsorption and re-emission process, so the measured lifetime appears longer than it really is. This process is especially strong in quasi-three-level lasers, since the fluorescence arises from the transition from the upper to the lower laser level. Since the lower laser level is also the ground state, it will always be populated, and re-absorption will be much more likely than in the case where the lower laser level is continuously depopulated, as in three-level or four-level lasers.

There are several ways to circumvent this error. Measuring lifetimes in samples of low doping concentrations lessen this effect, since fewer atoms can re-absorb the emitted fluorescence. Also, the crystals used have a high refractive index, around $n = 2$, allowing photons with a relatively large internal incidence angle to be reflected back into the sample instead of transmitted out to the detector. To avoid this, one can use a surrounding medium other than air with a matching refractive index, effectively reducing the internal reflections within the crystal.

7.2 Measurements

To properly investigate the Er-Yb system there are a number of lifetime measurements that have to be made. To investigate the forward/back transfer efficiency it is important to only pump the Yb system. That way, all fluores-

cence detected from the Er atoms is known to originate as absorbed pump radiation by the Yb atoms. By measuring the lifetimes of $^4I_{11/2}$ in Er and $^2F_{5/2}$ in Yb it is possible to estimate the forward transfer efficiency. Ideally, the $^2F_{5/2}$ lifetime should be long compared to the $^4I_{11/2}$ lifetime, making forward transfer more likely than back transfer, since the $^4I_{11/2}$ depopulates quickly. First, crystals doped only with Er or Yb were studied, to measure their intrinsic properties. Later, co-doped Er-Yb samples were studied to investigate the fluorescence dynamics.

7.3 The measurement set-up

The set-up for measuring the Yb, Er and co-doped crystals are very similar, so only the Yb and co-doped measurement set-up will be described in detail (since they are identical), whereas only the changes from the Yb set-up will be described for the Er measurement set-up.

The Yb and co-doped systems were pumped at around 935 nm, generated by an OPO pumped by a frequency doubled Nd:YAG at 532 nm. Since there are only two electronic levels in the Yb system, the pump wavelength is roughly the same as the measured fluorescence wavelength, so filters cannot be used to separate the fluorescence from the strong pump signal. To overcome this problem the fluorescence was measured perpendicular to the pump direction. A schematic of the set-up can be seen in Fig.(7.2). The pump for the OPO is a frequency doubled Nd:YAG so there are both 1064 nm and 532 nm components in the pump light, however the 1064 nm component is absorbed by a filter. The measured power of the 532 nm beam was 40 mW. A lens then focuses the pump into the OPO, which outputs a signal at 935 nm with a power of 10 mW, and consequently an idler at 1234 nm, and a measured power of around 2.5 mW. The OPO is tunable by either rotating or changing the temperature of the nonlinear crystal, PPKTP, inside the cavity. In all set-ups used in this thesis the PPKTP was rotated at an angle with respect to the pump beam. Due to phase-matching con-

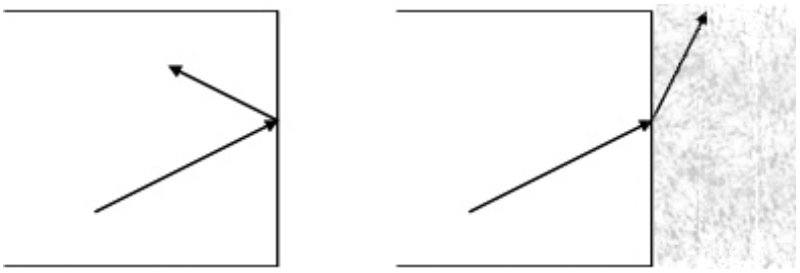

Figure 7.1. *By changing the refractive index in the surrounding medium internal reflections can be reduced.*

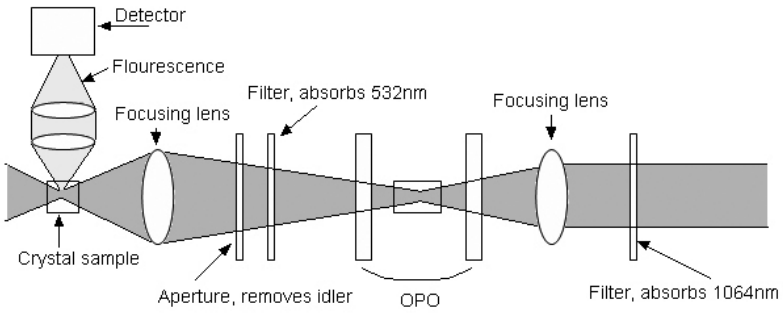

Figure 7.2. *The set-up used when measuring the Yb lifetime.*

ditions inside the PPKTP crystal, the signal and idler will exit the crystal at slightly different angles. This makes it easy to block the idler and let the signal pass. After the OPO there is a filter to absorb the remaining 532 nm pump, and an aperture to block the idler, but let the signal through. The signal is then focused to a 160 μm diameter spot in which the doped crystal is placed. Fluorescence is detected perpendicular to the pumping, where light is gathered and collimated by a microscope objective, after which it is focused onto a photodetector connected to an oscilloscope. The pump is pulsed with a frequency of 20 Hz and a pulse length of 3 ns. When measuring the Er doped samples, 532 nm was used to pump the system, because of the small cross section of Er at around 1 μm. Hence, the aperture and filter absorbing 532 nm was removed, as well as the PPKTP crystal.

Using Beer Lambert's law, the intensity is approximately halved after passing the crystal, which means that half the photons are absorbed in the crystal. For one pulse this corresponds to roughly 10^{15} excited ions, which is approximately one thousandth of the total ions in the crystal.

First, a test series of measurements were taken to ensure that the set-up worked properly. Only fluorescence around 1 μm was measured in this series, and the results can be seen in table 7.1. The results were in agreement

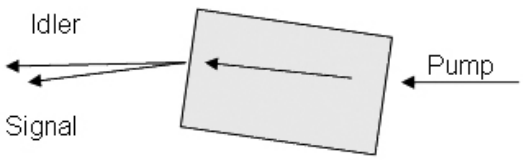

Figure 7.3. *The signal and idler will exit the crystal at different angles.*

Table 7.1. *Measurements*

Host crystal	Er conc.	Yb conc.	Lifetime [μs]
KGW	0.5%	5%	281
	0.5%	2.5%	237
	2.5%	7.5%	206
	5%	5%	158
	1%	-	118
	3%	-	136
	5%	-	146
KYW	0.5%	5%	291
	0.5%	2.5%	265
	5%	-	124
KLuW	5%	-	116
	3%	-	101
	0.5%	-	107

with previously measured lifetimes of the same crystals [10], so the set-up was assumed to be producing reliable results. However, no measures had been taken to reduce the effect of radiation trapping, which could be influencing the results. To get reliable results this also had to be taken into account. However, the methods of reducing radiation trapping previously described is not easily applicable to this set-up. Immersing the crystals in an index matching medium is not practical, and since measuring the fluorescence dynamics of the different crystals is the goal, it is not possible to measure crystals with low doping concentrations only. Another way of reducing radiation trapping had to be used.

7.4 Reducing radiation trapping by using a confocal microscope

In a paper produced by Petermann et.al. [11], it was mentioned that an aperture was used to reduce the effect of radiation trapping. There was no description of exactly how this was done, but since apertures and pinholes were available in the lab this could be a nice way to reduce radiation trapping. Through consultation with my supervisors, a few modifications were made to the set-up, which can be seen in Fig.(7.4).

By pumping the crystal at an angle, a major part of the excited dopants will be very close to or on the surface of the crystal. Fluorescence emitted in the direction of the detection system will have a much shorter distance to travel inside the crystal, if any, making re-absorption much less likely. The aperture is placed in the image plane of the two gathering lenses, whereby it is possible to choose the area from which the fluorescence is detected.

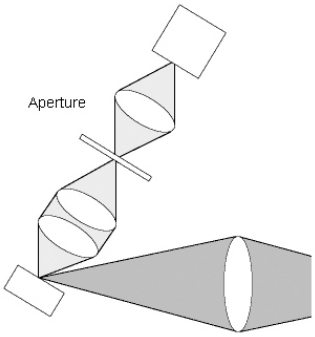

Figure 7.4. *The new set-up, employing a confocal microscope to reduce radiation trapping.*

This is the basic principle of confocal microscopy.[3] Fluorescence that is reabsorbed, re-emitted and then detected most often seem to have another point of origin than from the site where the pump photon was first absorbed, see Fig.(7.5). By placing the aperture in the image plane, see Fig.(7.4), it is possible to decrease the area from which fluorescence is detected without blocking the pump beam at the same time, which would reduce pump power. (Note that the effective aperture size is achieved by dividing the measured aperture diameter with the magnification factor of the detection system, since the aperture is placed in the image plane.) So, by measuring the lifetime for different aperture diameters, by extrapolating down to zero diameter it should be possible to get an estimate of the true lifetime, without any radiation trapping. To test whether this set-up would work at all, a test series of measurements was taken on a KYW crystal, doped with 5% Yb. In previous measurements, lifetimes around 440 μs has been reported for the very same sample [10], however other groups have reported lifetimes of 240–280 μs [11, 12], suggesting that radiation trapping is very prominent for this crystal and dopant, so this would make a suitable first test of the set-up. Nine measurements were made at aperture diameters ranging from 2–10 mm, and the result can be seen in Fig.(7.6).

As can be seen, there is a clear dependence between the aperture diameter and the measured lifetime. This set-up seems to reduce the radiation trapping, and can be used to get better estimates for all the doped crystals.

The original set-up was adjusted as described above and new series of measurements were taken. The procedure for this is outlined below:

[3]Confocal microscopy is primarily used to generate 3D or hi-resolution 2D images. Only imaging one point at a time by blocking light not in focus, or from other points in the focal plane, means that only information that "belongs" in a certain image point will reach it. However, the process of constructing an image is slow, since constructing the image point-by-point can be time consuming.

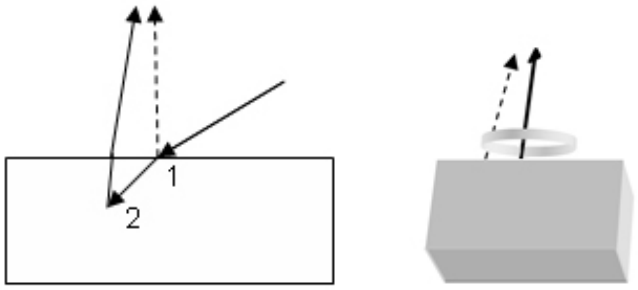

Figure 7.5. *A photon is absorbed at position 1, and the fluorescence therefrom is absorbed at position 2. The fluorescence from position 2 is then detected. If the fluorescence had been detected from position 1, it would have had a different point of origin than the re-absorbed fluorescence. The aperture blocks beams coming from a position off-centre. The smaller the diameter of the aperture is, the closer to the centre point the origin of the beams must be.*

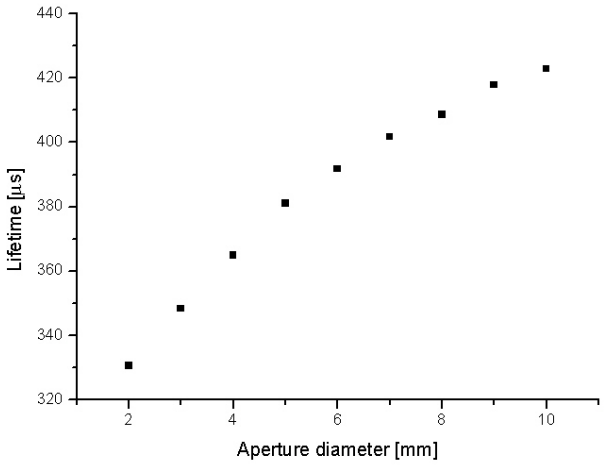

Figure 7.6. *The lifetime plotted against the aperture diameter for Yb5%:KYW, the first attempt using confocal microscopy.*

For every crystal 12 measurements were taken, with aperture values 10 mm – 3 mm in steps of 1 mm, and 2.5 mm – 1 mm in steps of 0.5 mm. Each measurement was taken on a digitized oscilloscope with a sampling rate of 2 GHz. An example of a lifetime measurement can be seen in Fig.(7.7).
In Fig.(7.7) a comparison showing the results when the lifetime is measured with different aperture settings can be seen.

7.5 Theory

Using a confocal microscope to reduce radiation trapping in measurements seems work, but what factors affect the function and applicability of this method was still not fully understood. For example, the measurements from two different crystals can be seen in Fig.(7.8). The method seems to reduce radiation trapping, but the behaviour is different for the two crystals, even though the same set-up has been used to reduce radiation trapping. To gain an insight to the processes at work, a model of how radiation trapping actually works was constructed and studied.

7.5.1 A random walk

As described above, the radiation trapping process is the absorption and re-emission of fluorescence photons by the dopants in the crystal. In a photon's perspective this can be thought of as a random walk in 3D, with a variable step size and delay between steps. However, to get a qualitative picture of the behaviour of this random walk, some simplifications were made to the model.

As will be discussed in section 8, the distance a photon travels in a medium is random, following an exponential distribution given by Beer-Lambert's law. To easily calculate the distance a certain photon has traveled, the Beer-Lambert law can be seen as the cumulative distribution function for the event of photon absorption. The probability density function describing the distance a photon travels in a medium of absorption cross section σ and doping concentration ρ can then be described as

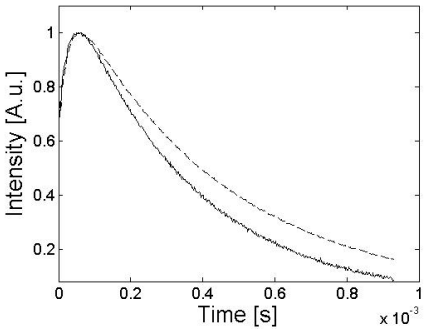

(a) Linear scale

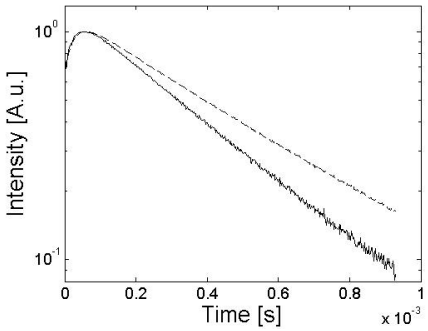

(b) The same measurements in semi-log scale.

Figure 7.7. *A comparison of two measurements from Yb5%:KYW taken with aperture diameters 10 mm (dashed line) and 2 mm (solid line). The shorter lifetime measured with the 2 mm diameter is apparent.*

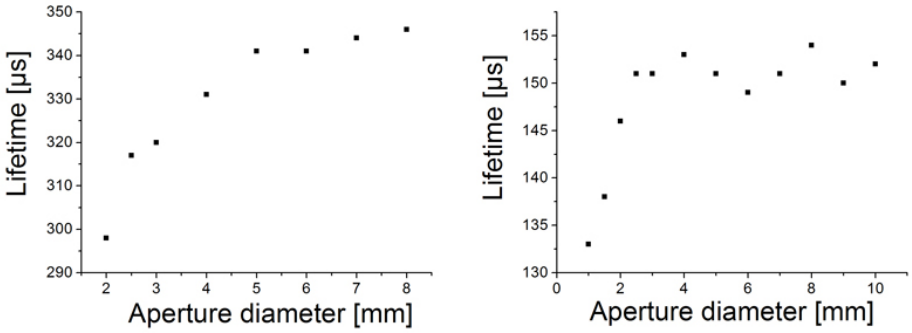

Figure 7.8. *The lifetime plotted against the aperture diameter for two different crystals, Yb5%:KYW and Er5%:Yb:5%:KGW.*

$$f(z) = \sigma\rho e^{-\sigma\rho z}.$$

From this, the average distance traveled by the photons in the medium can be calculated:

$$\langle z \rangle = \int_0^\infty z\sigma\rho e^{-\sigma\rho z}\, dz = \frac{1}{\sigma\rho}.$$

The random walk can thus be simplified by letting the step size be constant, with a value $1/\sigma\rho$. Also, the time delay for every step is set to one lifetime, τ.

To study the behaviour of this random walk, a simple program was constructed in MATLAB to simulate the outcome and results of many such events. A pump beam that is infinitely narrow travels in the positive z direction, and hits the crystal at the position $(0, 0, 0)$. It will travel a distance $1/\sigma_p\rho$ inside the crystal, where σ_p is the dopant's cross section for the pump wavelength. The random walk starts inside the crystal, after the pump photon has been absorbed the first time, see Fig.(7.9). For generality, all lengths are given in units of a fluorescence photon's step size, $1/\sigma\rho$. The starting point is then the ratio of the pump and fluorescence photon's average step size,

$$\frac{1/\sigma_p\rho}{1/\sigma\rho} = \frac{\sigma}{\sigma_p}.$$

The simulation traces a photon at a time, and stops it when it leaves the crystal, or after it has taken too many steps to be interesting. If the photon leaves the crystal at the surface, i.e. the plane $z = 0$, the point at which it crossed the surface is saved, as well as the number of steps taken. The

simulation was run for 100 000 photons, and the data from it is presented below.

7.5.2 Results from the simulation

The exact position of where the photons excited the crystal is not so important, but rather the *distance* from the origin, so when analyzing the results, the coordinate system is converted to cylindrical coordinates:

$$\begin{aligned} r &= \sqrt{x^2 + y^2}, \\ \theta &= \arctan\left|\frac{y}{x}\right|, \\ z &= z, \end{aligned}$$

see Fig.(7.10). Note that the θ angle is the angle in the first quadrant. If the point is not in the first quadrant a multiple of $\pi/2$ must be added.

A histogram showing how far from origin the photons exited the crystal in the plane $z = 0$ can be seen in Fig.(7.11). Since radiation trapping is caused by photons that have taken more than one step to get to the surface, it is of interest to see how the photons are distributed with the number of steps taken, since this effectively determines the amount of radiation trapping at different distances from the centre. The histogram in Fig.(7.11) is thus divided into sections, depending of the number of steps taken, which can be seen in Fig.(7.12). In this example, a little more than half of the photons that cross the surface $z = 0$ have done so in just one step. The curious hump that appears in the histogram is explained by the photons that have traveled to the surface in two steps. Their distribution from the origin can be seen in Fig.(7.13). The characteristics of this plot can be understood by looking at *how* the photon exits the crystal. In Fig.(7.14) a schematic of the photon paths that result in them crossing the surface in two steps is shown. Naturally, a photon that takes two steps and exits

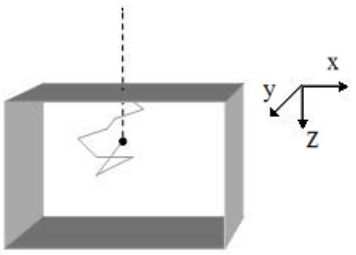

Figure 7.9. *A schematic of the model used in the random walk simulation.*

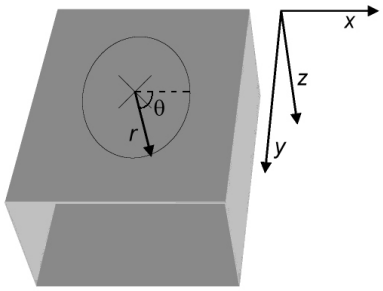

Figure 7.10. *A schematic showing the coordinate systems as defined in the simulation.*

the crystal cannot be farther away than two steps from the origin, and depending on the direction the photon took in its first step, it can exit the crystal in the interval indicated by the dashed lines in Fig.(7.14). A large number of photons cannot exit the crystal near the origin, or at a distance close to two step sizes, but most of them have a definite chance of leaving the crystal at around one step size from the origin, hence the slightly odd looking histogram.

The equivalent of radiation trapping in this model is thus how many steps it takes for a photon in its random walk to exit the crystal. The interesting thing to look for is then the average number of steps taken by the photons, since this will represent the measured radiation trapping. First, the average number of steps is plotted as a function of distance from the centre, which can be seen in Fig.(7.15). There seems to be a near linear dependence between the average steps taken and the distance from the cen-

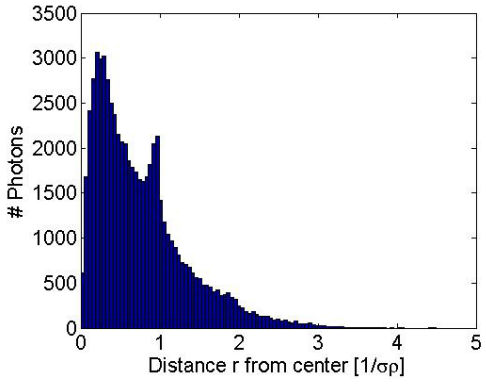

Figure 7.11. *A histogram showing how the photons leaving the crystal (at $z = 0$) are spatially distributed.*

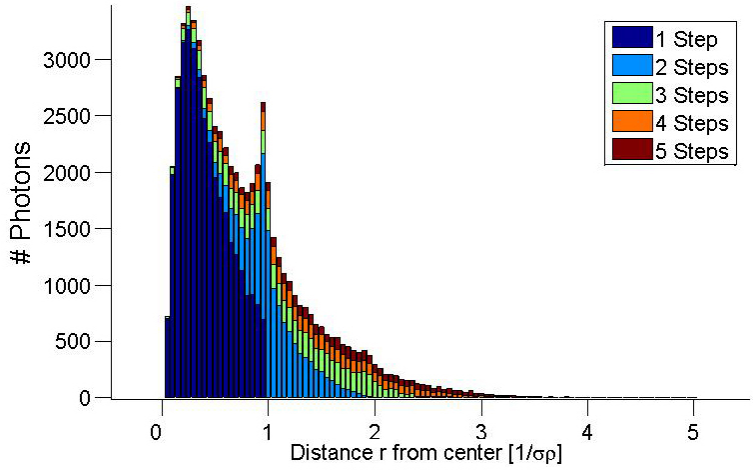

Figure 7.12. *The histogram again, now divided into number of steps taken by the photon when it hits the surface, starting with one step in the bottom layer and increasing.*

tre. In Fig.(7.16) a cumulative average is taken, so that the height of the graph at distance r represents the average steps taken by the photons that hit the crystal surface *within* a distance r from the centre. This is what is measured using the confocal microscopy set-up. The measured lifetime is proportional to the number of times the photons have been absorbed and re-emitted inside the crystal, so this curve answers some questions.

The plots in Fig.(7.6) show different behaviour when the same set-up has been used to try to limit the radiation trapping. However, in

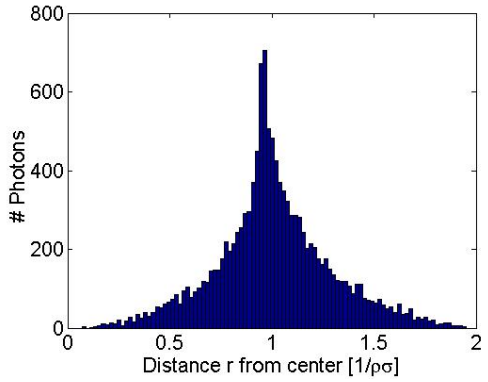

Figure 7.13. *The distribution of photons that crossed the plane $z = 0$ in two steps.*

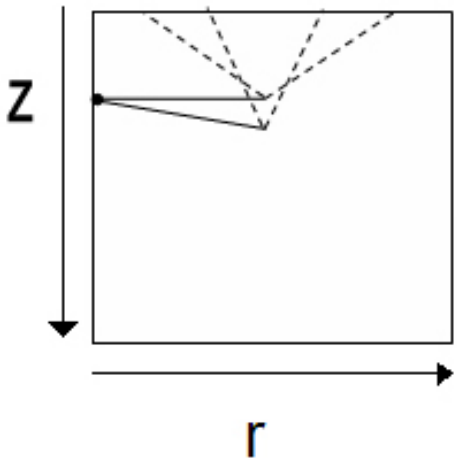

Figure 7.14. *A schematic showing how the photon can cross the surface in two steps. The dashed lines indicate in what interval the photon can hit the surface in two steps depending on the direction it took in the first step.*

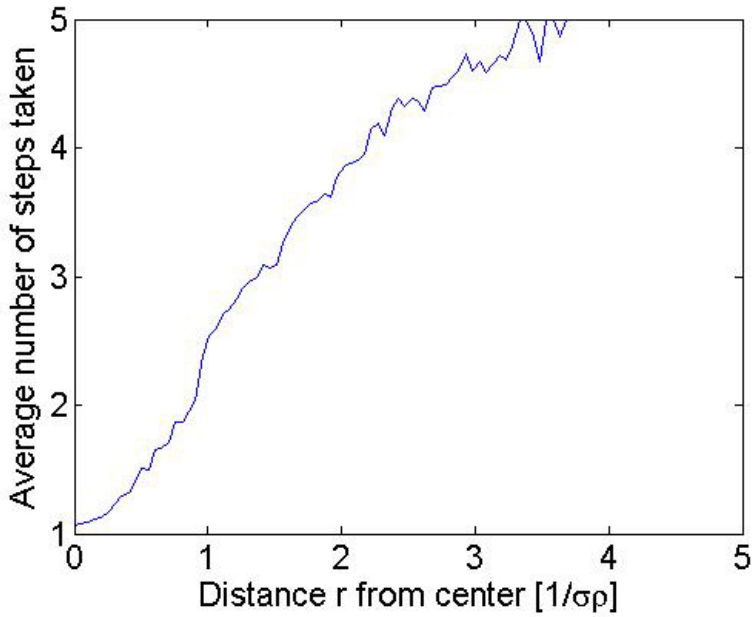

Figure 7.15. *The average number of steps taken as a function of distance from centre. The average steps taken seem to have a near linear dependence with distance.*

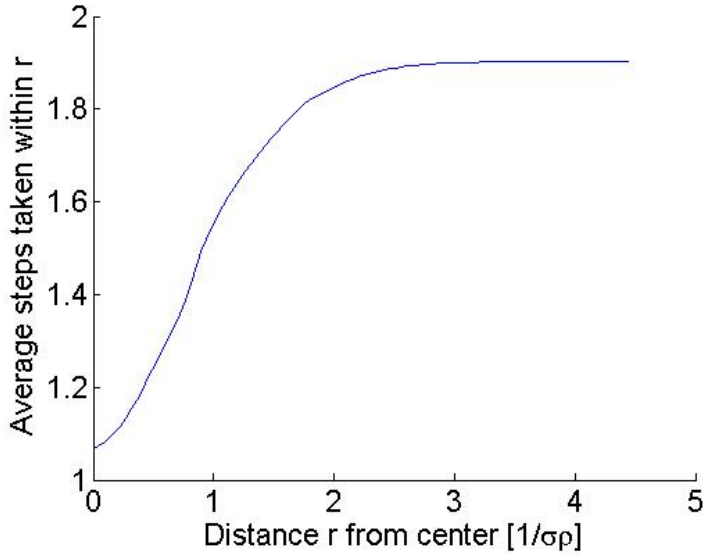

Figure 7.16. *The average number of steps taken within r as a function of r.*

light of the results from the simulation this can be accounted for. In Fig.(7.16), the distance from the centre is given in units of step-sizes, which is different for different crystals. In the crystal that is Er and Yb co-doped, Er5%:Yb5%:KGW, the average step size for a fluorescence photon is $1/\left(\sigma_{Er}\rho_{Er} + \sigma_{Yb}\rho_{Yb}\right)$, which is shorter than for the crystal doped with only Yb, Yb5%:KYW, where the step size is $1/\sigma_{Yb}\rho_{Yb}$. As a consequence, when using an aperture with a radius in the range of 1 mm to 5 mm for differently doped crystals, different parts of the graph in Fig.(7.16) will be obtained, see Fig.(7.17). For example, assume that the step size for the Er5%:Yb5%:KGW crystal is 1 mm, and 2 mm for the Yb5%:KYW crystal. When using an aperture with a radius in the range 1 mm – 5 mm, it is possible to see around five step sizes from the centre for the Er5%:Yb5%:KGW crystal, but only a little more than two step sizes for the Yb5%:KYW crystal. Thus, even if the graph would look the same if aperture radii were taken in the same interval with regards to step sizes for the two crystals, when the used aperture radii is in the same interval given in mm, the graphs look different.

Note that the measurements shown in Fig.(7.8) utilize different aperture diameter intervals, due to the fact that the signal was too low for any measurements to be taken at aperture diameters smaller than 2 mm for the Yb:KYW crystal. Also, since this model is just a crude first approximation, no real values should be calculated from this example. However, the

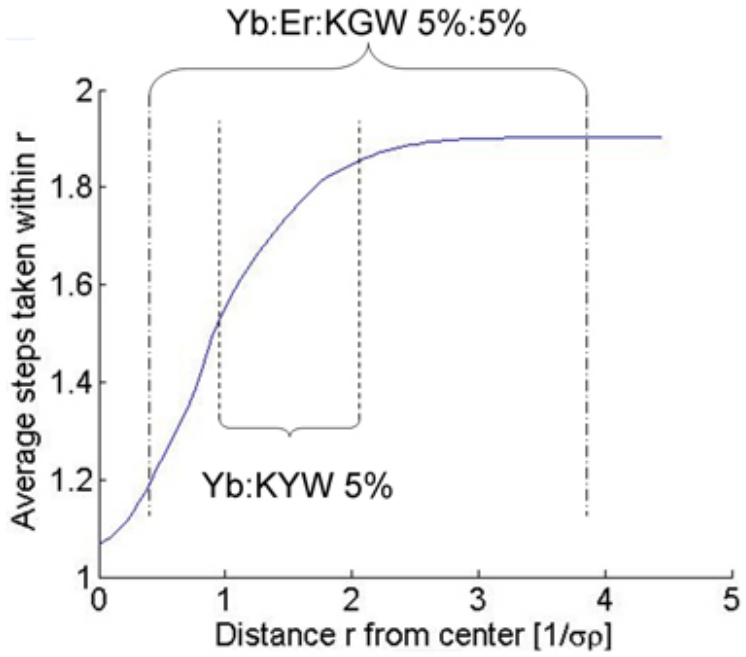

Figure 7.17. *The portions of the graph that can be seen in the lifetime measurements of Fig.(7.6).*

qualitative results still hold and seem to give the answers to some of the questions that arose when the results from the aperture measurements were first analyzed.

For this basic first simulation there are two variables that affect the outcome, the starting position and the number of steps taken before the photon is terminated by the program. As mentioned above, the starting position is just the ratio of the absorption cross sections for the pump and fluorescence photons. The maximum number of steps allowed before a photon is terminated is basically determined by the amount of radiation trapping in the crystal. When a lifetime measurement is taken in the lab, the time span after the pump pulse has excited the dopants is set to about 2–3 lifetimes, see Fig.(7.18), in order get reliable data. At large apertures and with high radiation trapping, the apparent lifetime could be twice or three times the real lifetime, so in some cases a photon might take up to nine steps before hitting the detector and being detected. These variables determine the shape of the cumulative average curve seen in Fig.(7.16), and the effect of these properties when taking measurements are outlined below.

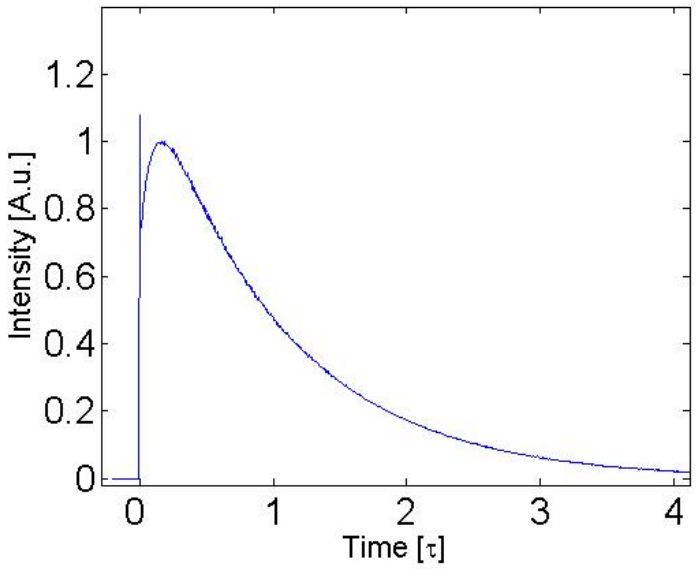

Figure 7.18. *A measurement of the fluorescence dynamics in Er0.5%:Yb2.5%:KYW, with time given in units of lifetimes.*

7.5.3 The starting point

The staring point determines how far from the surface the random walk starts. The farther into the crystal the pump photon is first absorbed, the more radiation trapping will affect the results. The result different starting points will have on the general shape of the cumulative average curve can be seen in Fig.(7.19), where the starting point rages between 0.1 and 1.1 step sizes, in steps of 0.2 step sizes. As can be seen, if the starting point is close to the surface, i.e. if the step size of the fluorescence photon is large compared to the pump photon, a linear extrapolation from the measured values closer than about one step size to the centre can give a decent estimate of the true lifetime. However, if the starting point is deeper inside the crystal, this method will not yield a good result and should not be used. The closer to the surface the pump beam is absorbed, the less radiation trapping there will be, and the easier it will be to estimate the true lifetime. One way of achieving this is by letting the pump beam hit the crystal at an angle, as described in section 7.4.

7.5.4 Number of steps taken

The other variable that determines the general shape of the cumulative average curve is the number of steps taken before the simulation terminates

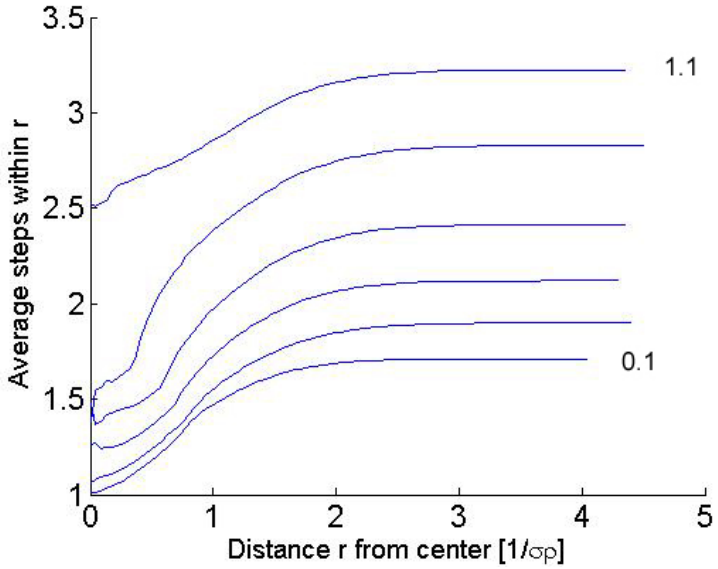

Figure 7.19. *A comparison of curves with different starting points, ranging from 0.1* $1/\sigma\rho$ *in the bottom, to 1.1* $1/\sigma\rho$ *at the top.*

the photon. If the amount of radiation trapping is high, there will be more steps taken by photons, on average. A comparison of curves with a constant starting point, and number of steps allowed for a photon before termination ranging from 2 to 8 steps, can be seen in Fig.(7.20). As can be seen, a linear extrapolation down to zero radius will give good results if the number of steps taken is within a measurement is five steps or more.

7.6 Interpreting the measured results

As explained above, a linear extrapolation down to zero radius will give a decent estimate of the true lifetime in some situations, but not all. The crucial factor here seems to be the starting point, or to be more accurate the depth at which the pump beam is absorbed and the random walk starts. When analyzing the results from the measurements, for most crystals there seemed to be a linear dependence between the aperture radius and the measured lifetime. An example of this is the Er0.5%:Yb5%:KYW, which can be seen in Fig.(7.21). The linear regression suggests a lifetime of 229 μs, and comparing this to the result achieved without the confocal microscope of 291 μs, see table 7.1, means a 21% decrease of the measured lifetime, due to elimination of radiation trapping.

However, some of the results did not show a simple linear behaviour, like the crystals in Fig.(7.7). These results had to be given some further analysis to properly determine the true lifetime. Three examples of measurement

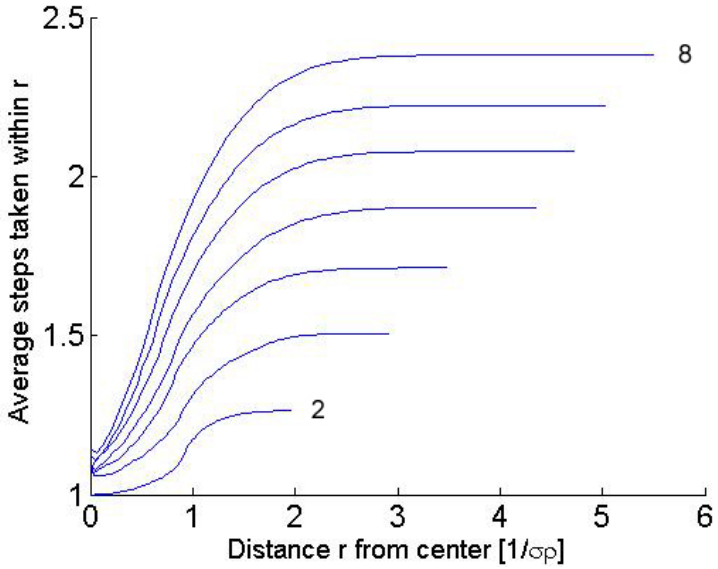

Figure 7.20. *A comparison of curves where the maximum number of allowed steps taken before a photon is terminated ranges from 2, the lowest curve, to 8, the one on top.*

data compared to the basic random walk simulation are presented below, where the simulation result has been fitted to the sampled data. Fig.(7.22) shows the measurements taken on the Er5%:KGW crystal, pumped at 532 nm, and the measured fluorescence at 1 μm. This curve shows a somewhat different behaviour, with a steep drop at large apertures, which level out as the aperture size decreases. This behaviuor seems very similar to a random walk where the photon is terminated after just two steps, and with a quite shallow starting point, see the bottom graph in Fig.(7.20). Fitting the simulation result with the measured data show good agreement, and by studying the behaviour of the simulation one can draw the conclution that the true lifetime will be close to the lifetimes measured at small apertures. In Fig.(7.23) the measurements from Er1.4%:Yb2.5%:KGW can be seen, together with a random walk simulation in which the photons are terminated after eight steps, and have shallow starting position. A similar curve can be seen in Fig.(7.24), in which a random walk simulation of maximum five steps have been fitted to the measurements from the Er5%:Yb5%:KGW crystal.

The curves that are generated from the random walk simulations show a strong resemblance to the acquired data, implying that the random walk model works well. However, the simplifications made when implementing the model to simulations are of such nature that no quantitative results should be drawn from the results. I.e. the step size used in the simula-

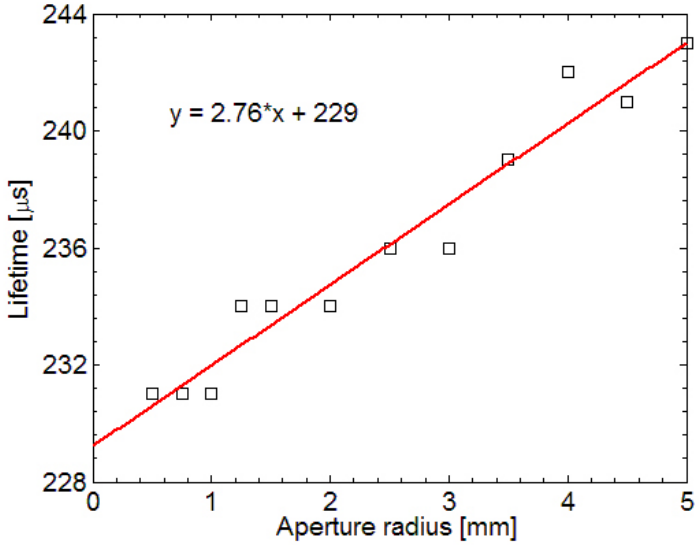

Figure 7.21. *Lifetime measurements of Er0.5%:Yb5%:KYW using a confocal microscope to reduce radiation trapping. A least squares linear approximation has been performed, which is presented as the line in the graph, and the equation is given.*

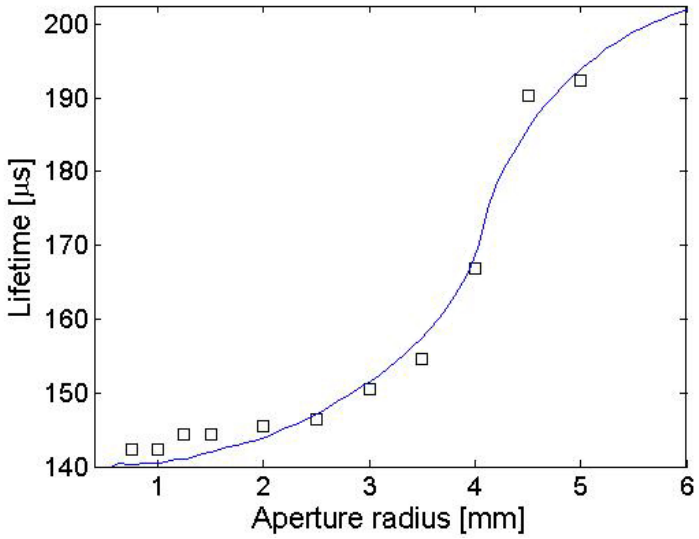

Figure 7.22. *Measurements from the Er5%:KGW crystal, compared to a random walk simuation.*

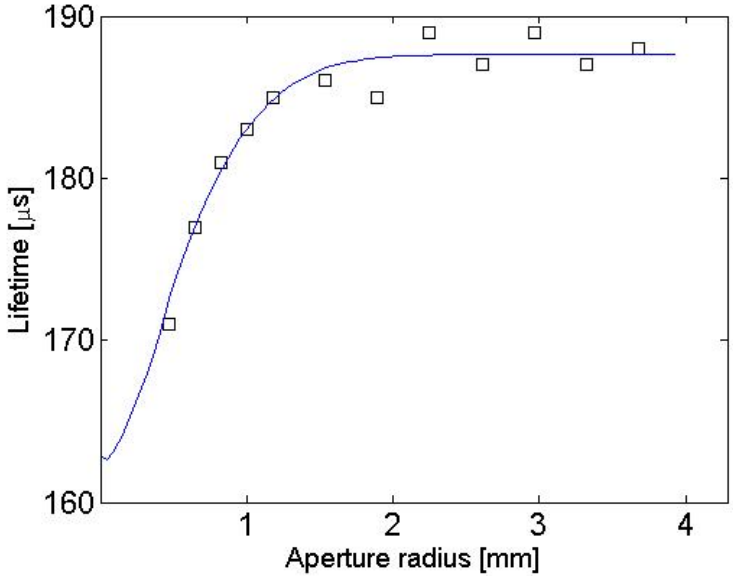

Figure 7.23. *Measurements from the Er1.4%:Yb2.5%:KGW crystal, compared to a random walk simulation.*

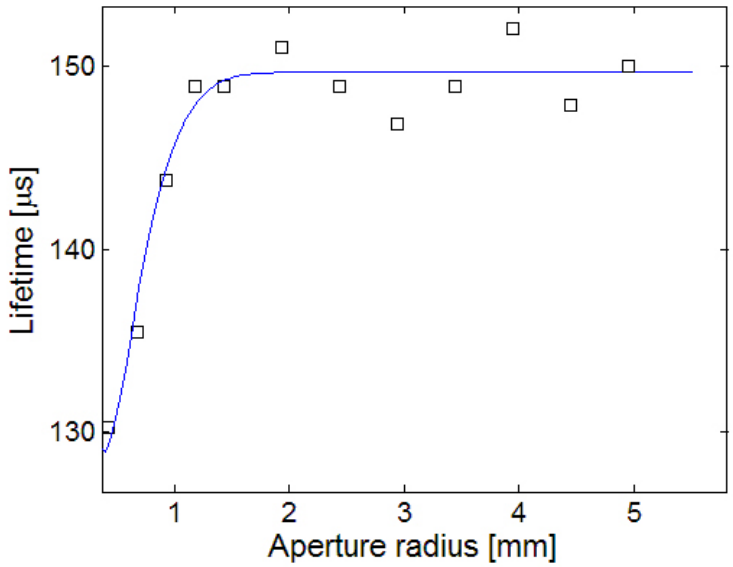

Figure 7.24. *Measurements from the Er5%:Yb5%:KGW crystal, compared to a random walk simulation.*

tions should not be calculated for the crystals for a direct comparison, but the simulations should only be used to study the general behaviour of the radiation trapping. The simplifications that step size and time delay are constant, the direction of the emitted photons is isotropic, together with the neglecting of other optical properties in the crystals such as internal reflection and refraction at the boundaries will make numerical comparisons erroneous. The simulation results that are fitted to the measured data in Fig.(7.22) to Fig.(7.24) are simply overlaid to show the good resemblance and the accuracy of the predicted behaviour of the results, not to get numerical values for the simulation variables or precise values for the true lifetime in the measurements. Still, conclusions can be drawn from the behaviour of the simulations, and can suggest ways of estimating the true lifetime from the measurements.

7.7 Results

Table 7.2 shows the lifetimes obtained when the means of reducing radiation trapping described in this section have been used, and a comparison to the results obtained when no measures were taken are made. The lifetimes are reduced by 10 – 40%, depending on the crystal and dopant. Table 7.3 shows the lifetimes obtained when using the confocal microscopy set-up to measure the $^4I_{13/2}$ transition in Er, with a fluorescence wavelength of around 1.5 μm. Very little radiation trapping was expected for this wavelength, so no reference measurements were taken in the initial set-up. To still be able to make som kind of comparison, the maximum value obtained in a measurment series was taken as reference, usually the value obtained at maximum aperture. However, the value obtained at maximum aperture is not necessarily the value obtained when no aperture is used at all, so the percental decrease is a lower limit of the true value. The measurment series showed the same type of behaviour as measurement series in the 1 μm region suffering from radiation trapping, so the same methods for calculating the true lifetime were applied.

In section 4, a relation connecting the lifetimes, forward- and back-transfer rates and the doping concentrations was derived, Eq.(4.18):

$$W_{eff,2} \approx 1/\tau_{Yb} + \frac{\gamma_{nr,3} - 1/\tau_{Yb}}{1 + (W_{FT}/W_{BT})^{-1}} \Rightarrow \tag{4.18}$$

$$1/\tau \approx 1/\tau_{Yb} + \frac{1/\tau_{Er} - 1/\tau_{Yb}}{1 + \left(\frac{k_{FT}}{k_{BT}}\frac{[Er]}{[Yb]}\right)^{-1}}. \tag{7.1}$$

Eq.(4.18) has been clarified in Eq.(7.1), where τ is the measured lifetime in the co-doped crystals. τ_{Er} is the lifetime measured for the $^4I_{11/2}$ level, this

decay is principally governed by the non-radiative decay rate $\gamma_{nr,3}$, since it is much quicker than the fluorescence decay rate, which is why it can be substituted into Eq.(7.1). Similarly, τ_{Yb} is the measured lifetime of the Yb-doped crystal. By making a least-squares fit of this equation, an estimate of the ratio k_{FT}/k_{BT} can be made. In Fig.(7.25) two graphs showing the measured lifetimes plotted against the [Er]/[Yb] ratio can be seen, together with the least-square fit of Eq.(7.1). The resulting ratio of the forward and back transfer was $k_{FT}/k_{BT} = 4.2$ for the KGW crystal, and $k_{FT}/k_{BT} = 1.9$ for the KYW crystal. Previous calculations based on measurements where no attempts to reduce radiation trapping were made, see table 7.1, yield a similar result for the KGW crystal, $k_{FT}/k_{BT} = 4.2$, but a higher value for the KYW crystal was achieved, $k_{FT}/k_{BT} = 2.3$ [10].

In the least-squares fit, the lifetime of the Er5%:Yb5%:KGW was omitted. This is due to the unreasonably low lifetime value of 124 μs, which is actually lower than the Er:KGW lifetime of 142 μs. As can be seen in Eq.(7.1), the curve tends asymptotically to the Er:KGW lifetime. This is because the upper Yb level, from which the detected fluorescence is emitted, will be depleted both through fluorescence and forward transfer. The rate of forward transfer is principally set by the decay rate of the corresponding Er level, $^4I_{11/2}$, and since this decay is faster, the upper Yb level lifetime will tend towards this value as the [Er]/[Yb] ratio increases. The reason for the low lifetime values measured for the Er5%:Yb5%:KGW crystal is unclear.

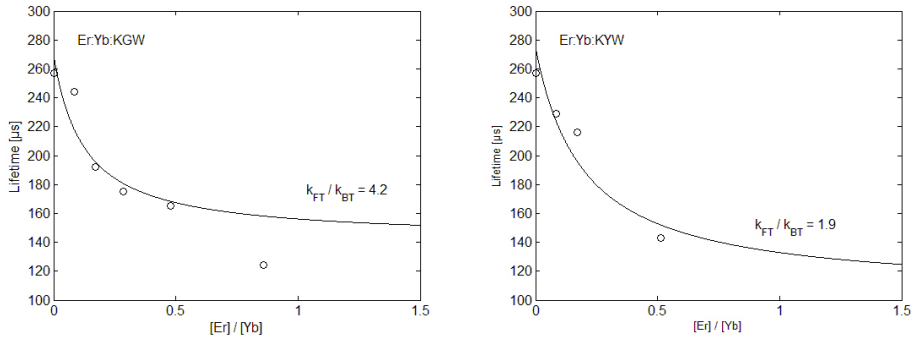

(a) *Lifetimes in KGW.* ***(b)*** *Lifetimes in KYW.*

Figure 7.25. *Measured lifetime vs. doping concentration ratio [Er] / [Yb] in KGW, (a), and KYW, (b).*

7.8 Summary and discussion

In this section, the problems of radiation trapping when performing lifetime measurements of energy levels in Er and Yb ions have been presented, along with ways of reducing them. One method, using a confocal microscope, has

Host crystal	Er conc.	Yb conc.	Lifetime, no aperture [μs]	Lifetime, aperture [μs]	Difference
KGW	0.5%	5%	281	244	13%
	0.5%	2.5%	237	192	19%
	2.5%	7.5%	206	175	18%
	1.4%	2.5%	212[a]	165	22%
	5%	5%	158	124	22%
	1%	-	118	-	
	3%	-	136	-	
	5%	-	146	142	3%
KYW	0.5%	5%	291	229	21%
	0.5%	2.5%	265	216	18%
	1.5%	2.5%	177[a]	143	19%
	5%	-	124	105	15%
	-	5%	440[a]	257	42%

[a]Value taken from measurements by Stefan Bjurshagen [10]

Table 7.2. *Lifetime measurements of fluorescence around 1 μm, which results from transitions from $^2F_{5/2}$ to the ground state in Yb and $^4I_{11/2}$ to the ground state in Er.*

Host crystal	Er conc.	$^4I_{13/2}$ lifetime, max. value [ms]	$^4I_{13/2}$ lifetime, calc. value [ms]	Difference
KGW	1%	3.12	2.92	6%
	3%	3.07	2.86	7%
	5%	2.67	2.39	10%
KYW	5%	3.16	2.16	32%

Table 7.3. *Lifetime measurements of fluorescence around 1.5 μm.*

been investigated and evaluated, both experimentally and theoretically using computer simulations, and the results from both the experiments and simulations indicate that the method is valid and reduces the effect of radiation trapping, whereby lowering the measured lifetimes with 10 – 40%. The method is simple to use and applicable to all host materials as well as dopants, which makes it suitable for characterization of crystals that is to be used in other set-ups. By analyzing the results from the simulations, the effect of using a confocal microscope to reduce radiation trapping can be studied and conclusions can be drawn as how to treat the measured data. For most crystal samples where the method was used, the results showed a linear depencece between the aperture radius and the measured lifetimes, where an extrapolation of the measurements down to zero aperture radius should give a rather good estimate of the true lifetime, without radiation trapping. A few crystals did not show a simple linear behaviour, and the result from these measurements have been presented together with simulations showing very similar behaviour, from which conclusions of how to estimate the lifetime without radiation trapping can be drawn. Even without the simulations infering how to treat the measured data, the raw data alone improves the result, reducing the measured lifetime with around 7 – 15% when comparing the results from the smallest aperture to the result where confocal microscopy was not used at all. Two crystals, Er1%:KGW and Er3%:KGW did not show a simple exponential behaviour in the measurements, so no clear conclusion can be drawn from these results, which is why they are omitted in table 7.2.

To understand the processes at work in greater detail, another simulation should be constructed where more factors and physical properties have been taken into account, increasing the accuracy of the results. Thus, a Monte Carlo simulation of the processes at work in radiation trapping was performed and compared to results from measurements. This will be described in the next section.

8 The Monte Carlo method

8.1 The basic ideas

The Monte Carlo method is a set of algorithms used in numerical simulations that use random numbers or pseudo-random numbers to simulate stochastic processes. In this thesis a Monte Carlo simulation is used to simulate the radiation trapping and energy migration/transfer processes in different crystals. In order to do this the simulation generates a photon at a time, and for every "choice" of events the photon encounters, like absorption, reflection, energy transfer and energy migration, a (pseudo) random number determines the outcome. Pseudo-random numbers are numbers which are statistically random, but which are generated by a deterministic process. I.e. a sequence of numbers appear to be random; there are no patterns or regularities, but it can be reproduced so the sequence is not truly random. Throughout this thesis, only pseudo-random numbers are used, but for simplicity they are referred to as "random numbers".

8.2 Modeling with random numbers

The random numbers ξ generated by the computer is uniformly distributed in the range $0 < \xi < 1$, however most processes are not uniform in their distributions. Take for example the task of randomly generating a distance of which a photon travels in a medium before it is absorbed. This is certainly not a value between 0 and 1, and it is not uniformly distributed either. There must be a way to convert a uniform distribution of numbers to the desired distribution for this to work. For a continuous distribution, the probability for an event to occur in the interval (a_1, b_1) is given by

$$P\left(a_1 \leq x \leq b_1\right) = \int_{a_1}^{b_1} f\left(x\right)dx, \tag{8.1}$$

where x is the random variable, e.g. the distance a photon travels before being absorbed, or the direction of which a fluorescent photon is emitted after being absorbed. $f\left(x\right)$ is known as the probability density function, or *pdf*, which defines the distribution of x over the interval (a, b). The *pdf* must fulfill two conditions:

- $f\left(x\right)$ must be greater than or equal to 0 for all x, $f\left(x\right) \geq 0 \; \forall \; x$,
- The area under the graph should be unity, $\int_a^b f\left(x\right)dx = 1$.

Similarly, the cumulative distribution function, *cdf*, is defined as

$$F\left(\chi\right) = P\left(a < x \leq \chi\right) = \int_a^{\chi} f\left(x\right)dx, \tag{8.2}$$

and gives the probability that x in the interval $a < x < \chi$.

In order to simulate a process, like the distance a photon travels, x should be randomly generated in (a, b), corresponding to $(0, \infty)$ for the photon. To use the randomly generated numbers ξ, a non-decreasing function $g(\xi)$ must be found that maps $\xi \in (0, 1)$ onto $x \in (a, b)$ one-to-one, i.e. $x = g(\xi), \xi = g^{-1}(x)$. This means that

$$P(g(0) \leq x \leq g(\xi_1)) = P(0 \leq \xi \leq \xi_1). \tag{8.3}$$

But from Eq.(8.2) this is just the *cdf* for the two different distributions, so it can be expressed

$$P(a \leq x \leq x_1) = P(0 \leq \xi \leq \xi_1) \Rightarrow F_x(x_1) = F_\xi(\xi_1), \tag{8.4}$$

where F_x represents the *cdf* for the variable x and F_ξ represents the *cdf* for the ξ variable. The random numbers ξ are uniformly distributed, which means that the *pdf* is 1, and thus the *cdf* is $F(\xi_1) = \xi_1$. Using this in Eq.(8.4) yields:

$$F_x(x_1) = \xi_1 \Rightarrow \int_a^{x_1} f(x)dx = \xi_1. \tag{8.5}$$

So, to randomly generate x within a probability density function $f(x)$, it is possible to generate a random number ξ_1 and then solving for x_1 in Eq.(8.5). This process has been clarified in Fig.(8.1) [13].

8.3 Photon propagation

In this section a brief overview of the rules and arguments for photon propagation using the Monte Carlo method will be presented.

8.3.1 The coordinate system

In order to do a proper simulation, a coordinate system must be defined. In the simulations all photons start at the crystal surface, inside the crystal. This is the X marked in Fig.(8.2), and has the coordinates $(0, 0, -1)$. The position of the photon inside the crystal is always given in this coordinate system, however it is not the only system used. To express the direction of the photon, a spherical coordinate system and a cartesian coordinate system are used, with the origin at the last position occupied by the photon.

8.3.2 Launching a photon

The photon is represented with a structure array, storing its position, direction and time inside the crystal, among other things. When a photon is launched, these values are set to their initial states, being position: $(0, 0, -1)$ and direction: $\left(0, \frac{\pi}{2}, 0\right)$ in a (θ, ϕ, r) coordinate system. Note that MATLAB

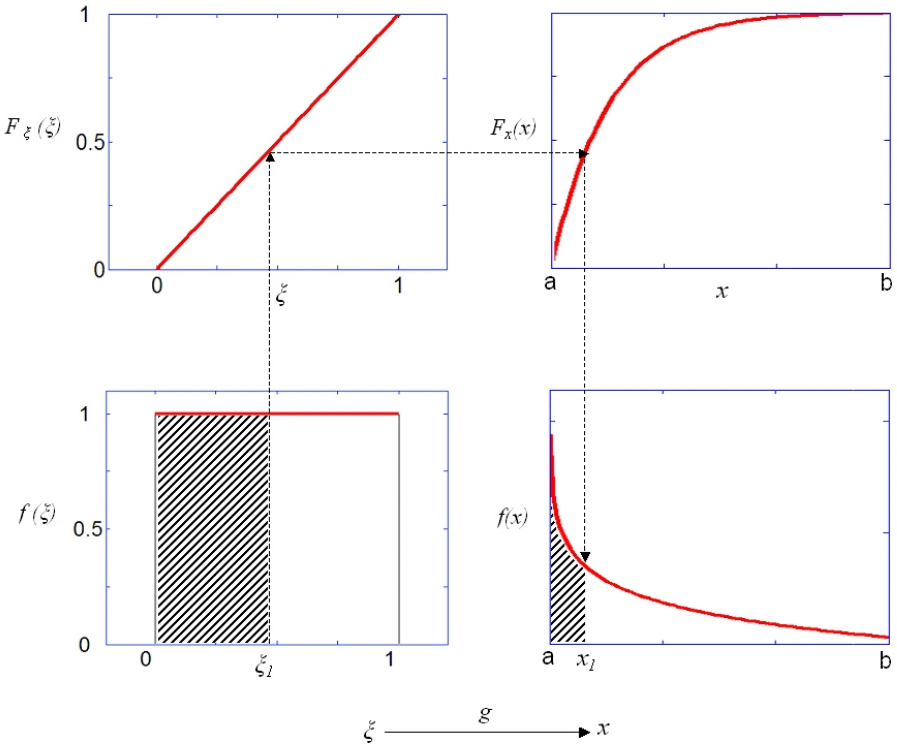

Figure 8.1. *The process of mapping a uniform distribution to another distribution, by setting the cdf's equal.*

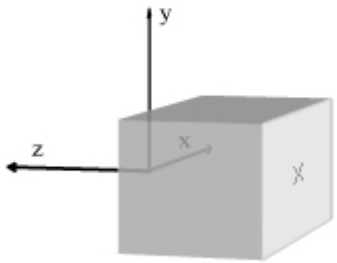

Figure 8.2. *The coordinate system in the simulation. The X marks where the simulation starts the photons.*

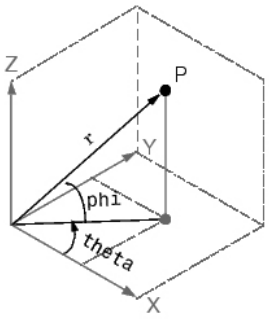

Figure 8.3. *The spherical coordinate system as defined in MATLAB.*

defines the spherical coordinate system as shown in Fig.(8.3), so the cartesian coordinates are defined as:

$$\begin{aligned} x &= r\cos(\theta)\cos(\phi), \\ y &= r\sin(\theta)\cos(\phi), \\ z &= r\sin(\phi). \end{aligned}$$

The photons are initiated inside the crystal, as a fraction of them would otherwise be reflected when hitting the crystal surface (11% or $\frac{1}{9}$ to be exact, if $n = 2$ in the crystal). This would only take up time and not contribute anything to the result.

8.3.3 Photon step size

After the photon has been initiated, the step size is calculated in the following way:

the intensity I of a beam traveling in the z direction that has traveled a distance l in a medium with particle density ρ, cross section σ and initial intensity I_0 is given by

$$I = I_0 e^{-\rho\sigma l}, \tag{8.6}$$

which is a form of Beer Lambert's law. Since the intensity is proportional to the number of photons, Eq.(8.6) can be rewritten as

$$\Phi = \Phi_0 e^{-\rho\sigma l} \Rightarrow \frac{\Phi}{\Phi_0} = e^{-\rho\sigma l}, \tag{8.7}$$

where Φ_0 is the initial number of photons and Φ is the number of photons after length l. The fraction $\frac{\Phi}{\Phi_0}$ is then the fraction of photons which has not been absorbed after distance l, or equally, the probability that a photon has not been absorbed after the distance l in the medium. The probability that

a photon *has* been absorbed is then:

$$P_{abs}\left(0 \leq z \leq l\right) = 1 - \frac{\Phi}{\Phi_0} = 1 - e^{-\rho\sigma l}. \tag{8.8}$$

As can be seen from Eq.(8.2) this is just the *cdf* for this event to occur. From Eq.(8.5) it is then possible to randomly generate a distance l traveled by the photon before being absorbed:

$$1 - e^{-\rho\sigma l} = \xi \Rightarrow l = -\frac{\ln\left(1-\xi\right)}{\rho\sigma} \equiv -\frac{\ln\left(\xi\right)}{\rho\sigma}. \tag{8.9}$$

In the last step it it recognized that $1 - \xi$ is equivalent to ξ, since ξ is uniformly distributed in $(0, 1)$. Eq.(8.9) is used every time a step size is calculated for a photon. The *pdf* can be calculated to be $f\left(z\right) = \sigma\rho e^{-\sigma\rho z}$ by differentiating Eq.(8.8), and can be recognized as an exponential distribution with rate parameter $\lambda = \sigma\rho$, which could be expected. An example of a mapping from a uniform to an exponential distribution can be seen in Fig.(8.4), where $\rho\sigma = 1\ \mathrm{m}^{-1}$ and $\chi = \rho\sigma l$.

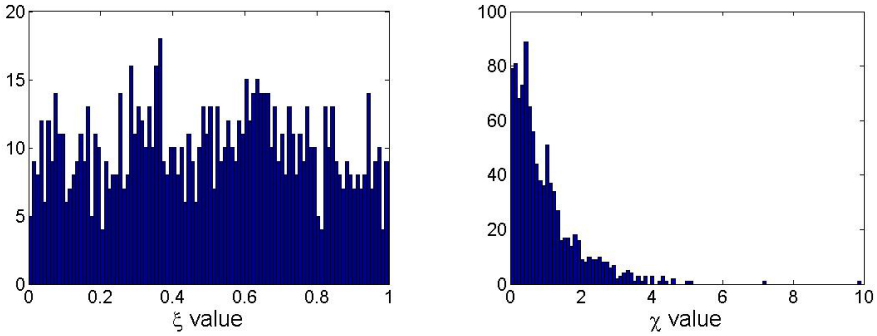

(a) *A uniform distribution of random numbers...* ***(b)*** *...mapped onto an exponential distribution.*

Figure 8.4. *The two histograms show 1000 random numbers mapped from a uniform to an exponential distribution. The height of the bars represent the amount of numbers; or for (b) photons, in the interval of the bar width.*

8.3.4 Absorption

After the photon has traveled the distance given by Eq.(8.9) it is absorbed by a dopant. This is no more dramatic than a decision of the next event and a time delay. The time delay is computed depending on the outcome, when the rate for the selected event is known. This is naturally also an exponential distribution, and the delay time is calculated as:

$$t = -\ln\left(\xi\right)\tau, \tag{8.10}$$

where τ is the lifetime. The derivation is virtually the same as for the photon step size so it will be omitted.

There are two general ways for the photon to continue, it can be re-emitted as fluorescence or it can be transferred to a neighboring atom through a non-radiative process, see section 5. The rate of decay is given by Eq.(5.7):

$$W_{tot} = \frac{1}{\tau_{rad}} + \frac{1}{\tau_{rad}} \sum_i \left(\frac{R_{DA}}{r_i} \right)^6 . \tag{5.7}$$

To use this equation the distances to the neighboring atoms must be known or estimated, and two different approaches have been made to do this.

8.3.4.1 Closest neighbour The first approach, which has some shortcomings, uses only the closest neighbour.

Since the non-radiative transfer falls off to the sixth power, only neighbours very close to the excited atom will be affecting the outcome. As a first approximation, only one atom will be considered, and its distance from the excited atom is randomly set using the nearest-neighbour distribution function $H(r)$, first considered by Hertz [14, 15]. He found that the distance to the nearest neighbour in a randomly Poisson distributed set of particles can be expressed as [14]:

$$H(r) = \rho \frac{d\upsilon_D(r)}{dr} e^{-\rho \upsilon_D(r)}, \tag{8.11}$$

where ρ is the particle density and υ_D is the volume of a D-dimensional sphere. For the 3-dimensional case $\upsilon_D = \frac{4\pi r^3}{3}$, so the expression for the closest neighbour becomes:

$$H(r) = \rho \frac{d}{dr} \left(\frac{4\pi r^3}{3} \right) e^{-\rho\left(\frac{4\pi r^3}{3}\right)} = 4\pi r^2 \rho e^{-\frac{4\pi\rho r^3}{3}}. \tag{8.12}$$

A graph of Eq.(8.12) can be seen in Fig.(8.5). The most probable distance for a neighbour to be found is

$$\begin{aligned} \frac{d}{dr}(H(r)) &= 0 \Rightarrow \left(1 - 2\pi\rho r^3\right) 8\pi\rho r e^{\left(-\frac{4\pi r^3}{3}\right)} = 0 \Rightarrow \\ 1 - 2\pi\rho r^3 &= 0 \Rightarrow r = (1/2\pi\rho)^{1/3}. \end{aligned} \tag{8.13}$$

By integrating by parts it can be shown that the *cdf* is

$$F(d) = \int_0^d H(r)\, dr = 1 - e^{\frac{4\pi\rho d^3}{3}}. \tag{8.14}$$

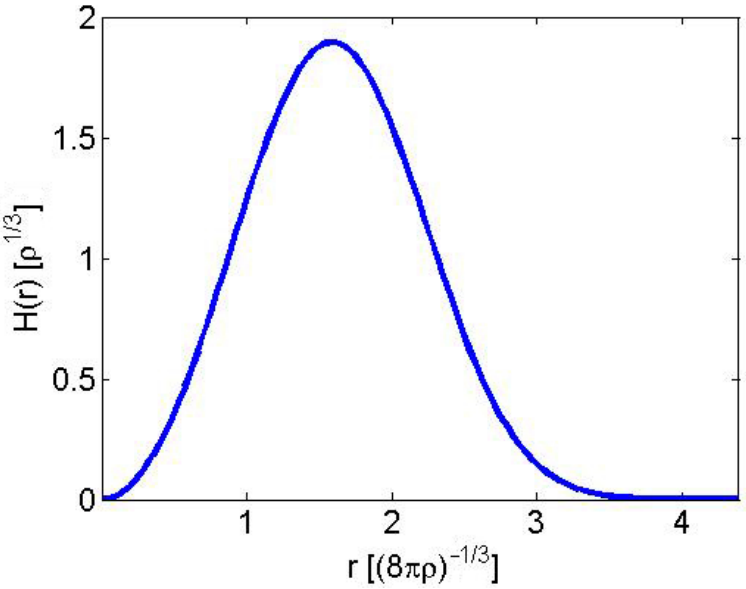

Figure 8.5. *The pdf for the nearest neighbour distribution. The distance* r *is given in the units of* $(8\pi\rho)^{-\frac{1}{3}}$ *and* $H(r)$ *is given in units of* $\rho^{\frac{1}{3}}$.

By again using Eq.(8.5) a randomly generated closest distance to a neighbour is given by

$$d = -\frac{3\ln(\xi)}{(4\pi\rho)^{1/3}}. \tag{8.15}$$

However, this model is not quite accurate in this situation; there are two main problems using this approach. Firstly, it only considers one neighbour. If the particle density ρ is high, there might be several neighbours within a Förster radius. If calculations are made on the assumption that only two events compete, fluorescence and energy transfer to *one* neighbouring atom, the fluorescence outcome will be erroneously favored. Eq.(8.16) describes the probability of the fluorescence event to occur in this model, whereas Eq.(8.17) describes the true probability.

$$P_{fluor} = \frac{1}{1+\left(\frac{R_{DA}}{r_i}\right)^6}, \tag{8.16}$$

$$P_{fluor} = \frac{1}{1+\sum_i \left(\frac{R_{DA}}{r_i}\right)^6}. \tag{8.17}$$

As can be seen in Fig.(5.2), if there are several neighbours with a distance $r_i > R_{DA}$ the true probability given in Eq.(8.17) can be significantly less than if only one neighbour is considered.

Secondly, this approach assumes that *any* distance to the closest neighbour is possible. However, the dopants are placed in a crystal lattice, so the distances between neighbouring atoms is a discrete set, whereas the closest neighbour approach assumes a continuous set. If the simulation was made for a glass host where the dopants are not constrained to lattice points, this would be the better suited model, under the condition that the doping concentration is sufficiently low that only one neighbour could be considered.

8.3.4.2 Array approach To address the shortcomings of the previous model, a second approach to this problem was made. To more accurately model the surrounding environment of the excited atom, a tree-dimensional array is generated, and each element represents a crystal lattice point. For simplicity the lattice can be assumed to be a simple cubic lattice, with a lattice constant a. By randomly placing atoms in the lattice points and then count the number of neighbours and their respective distance to the excited atom, the limitations of the first model are resolved. The implementation of this approach in the simulation is as follows:

When the photon is absorbed after a step size described above, a $7 \times 7 \times 7$ array of random numbers ξ_{ijk} is generated, where $i, j, k \in \{1 \dots 7\}$ represent the position of the random number in the array. Setting the excited atom in the $(4, 4, 4)$ position it is in the middle of the array, and the other elements represent neighbouring and close-by lattice points. By setting the doping concentration, the lattice points occupied by a dopant can be determined in the following way: assume that the doping concentration is 5%. This means that 5% of the acceptor sites are occupied by a dopant. From the $7 \times 7 \times 7$ array of random numbers, the elements fulfilling the condition that $\xi_{ijk} < 0.05$ are assigned as sites where dopants are present. By setting a value of the lattice constant a it is now possible to calculate the sum in Eq.(8.17) and thus getting a much more accurate

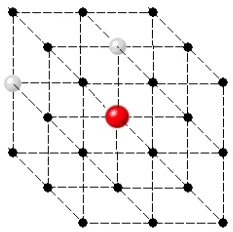

Figure 8.6. *A simplified example, showing a* $3 \times 3 \times 3$ *array, with the atom in position* $(2, 2, 2)$ *being the excited atom in question. There is one neighbour at distance* a *and one close-by atom at distance* $\sqrt{2}a$.

estimate of the outcome at each event. A simplified schematic can be seen in Fig.(8.6)

There are, however, some factors that need to be considered. Depending on the relative size of the lattice constant and the Förster radius, the size of the array may vary. If the Förster radius is smaller than the lattice constant, only the first or possibly two neighbouring "shells" can be considered, hence only a $3 \times 3 \times 3$ or $5 \times 5 \times 5$ array of random numbers have to be generated, whereas if the lattice constant is small compared to the Förster radius, more points will have to be considered in order to properly model the situation. In Fig.(8.7) the closest neighbour in units of lattice constants a can be seen for 10 000 randomly generated arrays, at a doping concentration of 1% and 15%. From Fig.(8.7*b*) it can be seen that the closest neighbour is at a distance

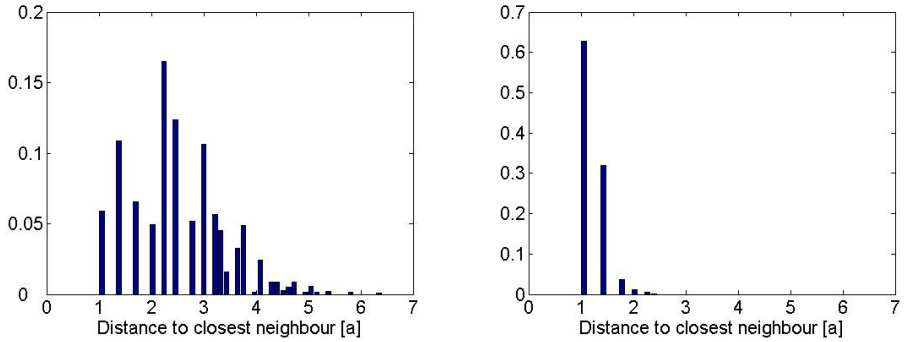

(a) *Closest neighbour at doping concentration* 1%.

(b) *Closest neighbour at doping concentration* 15%.

Figure 8.7. *The distance to the closest neighbour for 10 000 randomly generated environments at a concentration of* 1%*, (a), and* 15%*, (b). The height of the bars represent the relative abundance. The most probable distance to the closest neighbour is* $\sqrt{5}a$ *with around* 17% *at* 1% *doping concentration and* $1a$ *with around* 60% *at* 15% *doping concentration.*

of $1a$ in about 60% of the time. It is also worth mentioning that at 1% doping concentration there is statistically only about 2 other dopant atoms present in a $7 \times 7 \times 7$ lattice configuration. When doping concentrations are so low it is possible to see the multiplicities of the different lattice distances. For example, there are six sites at a distance $1a$ from the centre atom, but 12 sites at a distance of $\sqrt{2}a$ which can be seen in Fig.(8.7a), where the probability of the closest atom being at a distance $\sqrt{2}a$ is about twice as high as $1a$.

8.3.5 Emission

Using the expression for the different rates, the probability for each event to occur can be computed, and using a random number an event is chosen. When the outcome is determined, the delay time is generated, and the photon is moved. If the photon is emitted as fluorescence a new step size is determined, if energy transfer occurs the step size is already determined, and a new set of events has to be evaluated. The fluorescence emission is assumed to be isotropic, the direction is randomized. In order to separate the direction and the step size, the direction is generated in spherical coordinates. Generating a random direction in spherical coordinates is done by setting $\theta = 2\pi\xi_1$ and $\phi = \arcsin(2\xi_2 - 1)$, where ξ_1 and ξ_2 are two random numbers. The θ-coordinate is straight forward, but the ϕ-direction needs some explanation. From Fig.(8.3) it can be seen that $\phi \in [-\pi/2, \pi/2]$. To obtain a random number in $[-1, 1]$ one can use $\xi_{[-1,1]} = 2\xi - 1$, so to obtain a random number in $[-\pi/2, \pi/2]$ one can just multiply $\xi_{[-1,1]}$ by $\pi/2$. However, just letting ϕ be uniformly distributed in $[-\pi/2, \pi/2]$ generates a set of coordinates distributed over a sphere as can be seen in Fig.(8.8*a*). There seems to be a tendency for directions being generated in the polar regions, so it is not isotropic. To properly generate random directions, it is not ϕ

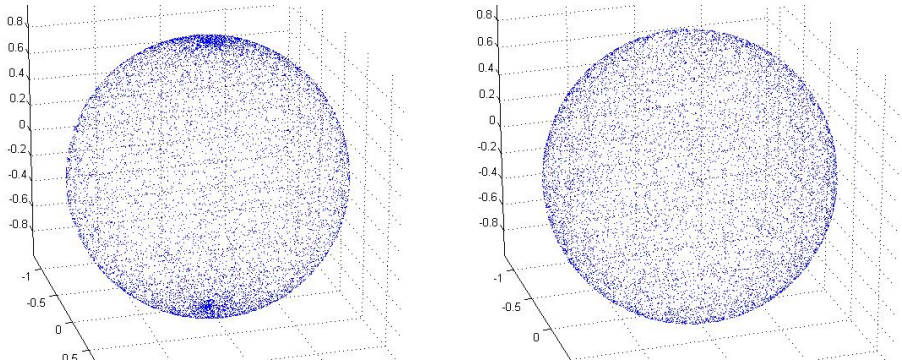

(a) *A uniform distribution of ϕ.* ***(b)*** *Correctly distributed ϕ.*

Figure 8.8. *A comparison of how two distributions of ϕ result in anisotropic and isotropic distribution of directions.*

that should be uniformly distributed, but rather the z-direction, which is given by $z = \sin(\phi)$. Since z is in the range $[-1, 1]$, a uniform distribution of z is then given by $z = 2\xi - 1$ and thus ϕ can be generated as

$$2\xi - 1 = \sin(\phi) \Rightarrow \phi = \arcsin(2\xi - 1), \tag{8.18}$$

see Fig.(8.8*b*).

8.3.6 Reflection and transmission at boundaries

During a step, the photon may hit the surface of the crystal. In this case it will be transmitted or reflected, based on the incident angle and the Fresnel equations [16]:

$$R_{\perp} = \left[\frac{\sin(\theta_t - \theta_i)}{\sin(\theta_t + \theta_i)}\right]^2, \tag{8.19}$$

$$R_{\parallel} = \left[\frac{\tan(\theta_t - \theta_i)}{\tan(\theta_t + \theta_i)}\right]^2, \tag{8.20}$$

where $R_{\perp}$ and $R_{\parallel}$ are the reflection coefficients for light perpendicular and parallel to the plane of incidence, respectively. By using Snell's law Eq.(8.19) and Eq.(8.20) can be rewritten in terms of θ_i:

$$R_{\perp} = \left[\frac{n_1\cos(\theta_i) - n_2\sqrt{1-\left(\frac{n_1}{n_2}\sin(\theta_i)\right)^2}}{n_1\cos(\theta_i) + n_2\sqrt{1-\left(\frac{n_1}{n_2}\sin(\theta_i)\right)^2}}\right]^2, \tag{8.21}$$

$$R_{\parallel} = \left[\frac{n_1\sqrt{1-\left(\frac{n_1}{n_2}\sin(\theta_i)\right)^2} - n_2\cos(\theta_i)}{n_1\sqrt{1-\left(\frac{n_1}{n_2}\sin(\theta_i)\right)^2} + n_2\cos(\theta_i)}\right]^2. \tag{8.22}$$

No polarisation of the light is assumed in the simulation, so the total reflection coefficient is given as a mean of $R_{\perp}$ and $R_{\parallel}$:

$$R = \frac{R_{\perp} + R_{\parallel}}{2}.$$

When a photon hits a surface, the total reflection coefficient is calculated. A random number ξ is generated, and if $\xi < R$ the photon will be reflected. Otherwise it will be transmitted through the surface, and its direction is changed according to Snell's law. If it passes the aperture and hits the detector it is registered as a detected photon. If not, the photon is killed and a new photon is generated.

8.3.7 Photon termination

There are a two ways in which a photon can be terminated in the simulation. First, it is killed when it exits the crystal. If it hits the detector it is registered first, then killed. The second way to end a photon is by a process called the roulette.

8.3.7.1 The roulette This process is used so that no photon lives forever, stuck reflecting between surfaces in a never-ending loop. Each photon is assigned a certain property called *weight*, with the initial value of $W = 1$. For every time the photon is reflected, the weight of the photon is multiplied with the reflection coefficient. After a certain number of reflections the weight will have decreased below a user defined threshold, e.g $W_{th} = 0.005$. To simply terminate the photon after a certain number of reflections would not be right, since it would not be done in an unbiased way. However, when it reaches the threshold, the photon enters a game of russian roulette. The game gives the photon one chance in m to survive, with a weight mW, else it is terminated. This way the photons are terminated in an unbiased way, yet they do not live forever.

These are the main processes that are the basis for the Monte Carlo simulation. In section 9 the implementation of these processes will be outlined, together with the construction of the programs and the data handling.

9 The implementation

The language chosen for the simulation was MATLAB, because of its ease of use and since my own experience in other languages are somewhat limited. With MATLAB one does not have to worry about memory allocation etc, and sub-routines and smaller functions can be constructed and tested separately in the command window. Also, the data output is very easily handled, and graphs can readily be produced to quickly see the results. Also, MATLAB's unique way of handling vectors and arrays greatly aided in the ease and simplicity of the coding process.

9.1 Model set-up

A few simplifications have been made from the experimental set-up used, see section 7.4. The photons come in at a right angle with the surface, and the detector is right in the virtual beam, see Fig.(9.1).

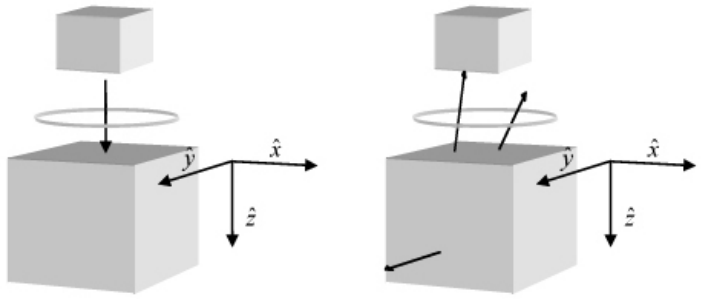

Figure 9.1. *A schematic of the set-up used in the simulation. The left figure shows where the photon enters the crystal. The right figure shows how photons might exit the crystal. There are two photons exiting the crystal at the top surface. Both pass the aperture, however only one hits the detector.*

For simplicity the optical system is neglected, and the detector is placed just after the aperture. The aperture is actually placed right on the surface of the crystal, but for clarity it is a separate entity in Fig.(9.1). Placing it on the surface is in effect the same as placing it in the image plane of the optical system.

9.2 Data handling

The central element in the simulation is the propagation of a photon, and how it interacts with the crystal. In the simulation the photon is represented with a structure array, storing the photon's necessary properties such as time inside the crystal, position, direction, wavelength etc. Every time a photon

is generated, a subroutine produces a structure representing a photon in the starting position, see Fig.(8.2). As the photon progresses in the simulation, the different posts in the structure are updated accordingly. In table 9.4 two structures representing photons in different stages are shown.

time:	0	time:	8.326844104103665e-004
weight:	1	weight:	0.16585955362095
dead:	0	dead:	0
host:	'Yb'	host:	'Yb'
pos:	[0 0 -1]	pos:	[0.84999 0.20956 0.20215]
dir:	[1x1 struct]	dir:	[1x1 struct]
bounce:	0	bounce:	3
node:	0	node:	1
wavelength:	935	wavelength:	1000

Table 9.4. *Two structures as they appear in the simulation. The initial photon to the left, and a photon in the middle of the simulation to the right*

Some post are self explanatory, but a brief summary of every post will be presented.

`time` gives the time the photon spent inside the crystal.
`weight` gives the *weight* of the photon, see section 8.3.7.
`dead` is a boolean variable. If one subroutine terminates the photon it will not be processed by other subroutines.
`host` stores the species of the host atom, Er or Yb.
`pos` stores the position in cartesian coordinates.
`dir` stores the direction of the photon in cartesian and spherical coordinates.
`bounce` counts how many times the photon has changed direction.
`node` counts how many hosts the photon has had.
`wavelength` gives the wavelength of the photon in nm, which can be either 935 for a pump photon, 1000 for a fluorescence photon from the $^2F_{5/2}$ in Yb or $^4I_{11/2}$ in Er, or 1550 from $^4I_{13/2}$ in Er.

9.3 Detection

When a photon hits the detector a number of variables are stored for analyzing the results and checking the simulation for bugs. The crucial variable here is the `time` variable. One method of storing the time information is to divide the time line into intervals or *bins*, and check in which bin the time from a certain photon would fall. Every bin holds an integer value, and at the end of the simulation the integers from every bin are collected, and a histogram can be made of how the photons were distributed over time. The output data would then be a vector of integer values, representing the bins. This approach is not very practical to use when many different simulations

are run and the lifetimes vary. The risk is that the temporal resolution would be too low, so that a majority of the photons would fall into one or a few bins, leaving little data to perform any calculations on. The method used in this simulation is simply to store the exact time of each photon's arrival at the detector. The output data is then a vector of floating points numbers. With this original data, a suitable resolution can be chosen and the data can be divided into appropriate time intervals to be analyzed.

9.4 Flowchart

Fig.(9.2) shows a basic flowchart of the simulation program. Many events describe processes already discussed in section 8. The first four boxes after the "Launch photon" box describes the event chain of the pump photon, which differs somewhat from the fluorescent photons that appear further down in the chart. The pump photon will not be detected if it leaves the crystal, as it is uninteresting for the result.

The "Launch photon" event launches a photon in the simulation, with the initial values as described above. The distance the photon travels in the crystal is determined in the "Set distance" box, based on Eq.(8.9). If the photon hits the crystal boundary it will either be reflected or transmitted. If it is reflected it goes through a game of russian roulette, if the weight of the photon is small enough. If it terminates there, or is transmitted, a new photon will be launched.

If the pump photon does not hit a boundary it is absorbed by a dopant. The absorption cross section, σ_{abs}, is changed, as is the photon property "wavelength", since they are different for pump photons and fluorescent photons. Before the photon leaves its host atom, the process in which it does so is determined, symbolized by "Decay process" in the flowchart. Based on the species of the host atom, as well as the proximity to other neighbouring and close-by atoms, the outcome is determined. If the photon is transferred through energy migration, a time constant is added, and the new position is stored in the structure representing the photon. If the photon is re-emitted as fluorescence, the decay time, direction and distance traveled before being absorbed is calculated, see section 8 for a description of how these values are determined If the photon is transmitted and hits the detector it will be registered as a detected photon.

9.5 Running the simulation

When running the simulation there are a number of input variables that need to be given to the program, which include the number of photons to be tracked, the aperture diameter, the cut-off time, Er and Yb doping concentration.

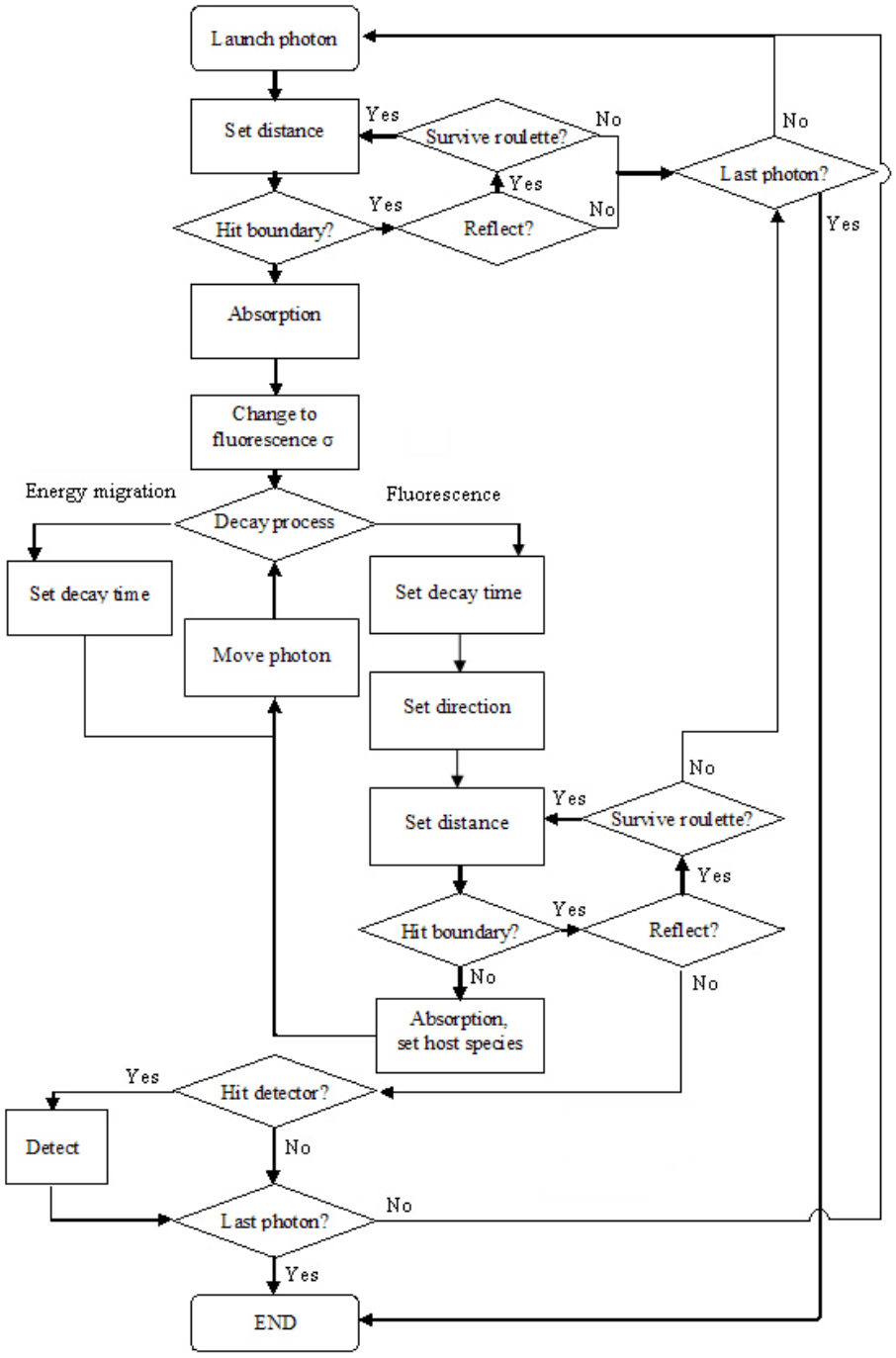

Figure 9.2. *The flowchart of the simulation, outlining the basic events.*

The number of photons is the amount of photons that are detected by the simulation, not the amount of launched photons. This is a better approach, since the number of detected photons would otherwise vary with aperture, giving simulations for different aperture values different accuracies. By setting the detected number of photons to a specific value for all apertures gives the same amount of data for any aperture. For most simulations, the detected photons have been set to 2000.

The cut-off time gives the time interval in which the photons will be tracked, and detected. This is very similar to the temporal resolution set on the oscilloscope when taking measurements.

There are variables that are set within the simulation, and are the same for crystals of different doping concentrations. These include absorption and emission cross section, Förster radii, lifetimes of the different energy levels and crystal dimensions.

The results from the simulations described here will be presented in the next section.

10 Simulation results

The results from the Monte Carlo simulations are presented here, and compared to the measurements as well as the simulations described in section 7.5.1.

10.1 Yb 5%:KYW — a comparison

The crystal that was first used when testing the confocal microscopy set-up described in section 7.4, Yb 5%:KYW, was the crystal that became the benchmark when comparing the results from the Monte Carlo simulation to the measurements. There were two reasons for this: first, there were pronunced radiation trapping in this crystal, making it a suitable first crystal to simulate since the effects would be easily seen if the simulation worked well. Secondly, the crystal is not co-doped, which means that the simulation could be tested without the energy transfer process fully implemented.

In order to simulate the radiation trapping process, the true lifetime of the transition must first be assumed, see Eq.(8.10), where the lifetime τ must be assigned a value in order to generate a delay time at all. This makes the Monte Carlo simulation a little different from the random walk simulation in section 7.5.1 in that the true lifetime must be guessed, and the results will indicate whether this guess is valid or not. The results from a series of simulations using a confocal microscope to reduce radiation trapping can be seen in Fig.(10.1), along with a comparison to measurements taken from the very first attempt using confocal microscopy.

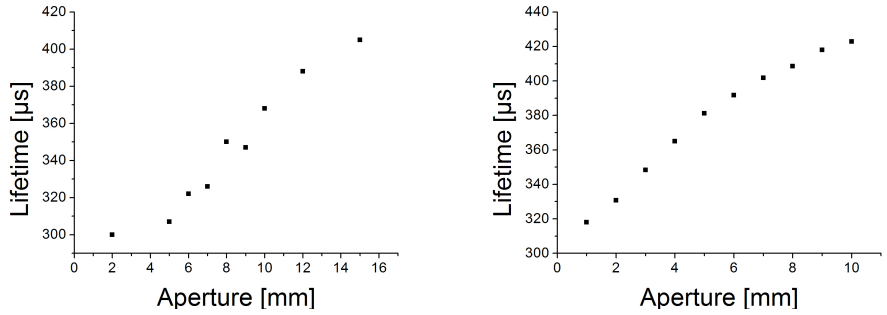

(a) *The result from the Mote Carlo simulation.* ***(b)*** *The results of the measurements.*

Figure 10.1. *A comparison between the measurements and the results from the Monte Carlo simulation.*

Apparently, the simulation seems to reproduce the results from the measurements quite well, even though the aperture diameters differ somewhat.

The discrepancies can be explained by slightly incorrect values of the dopant particle concentration, cross section and lifetime.

For even larger apertures, the lifetimes levels out in the same manner as the graphs from the random walk simulation in section 7, further confirming the models used.

10.2 Non-radiative energy transfers

In this simulation, the non radiative energy transfers were turned off for three reasons. First, this process will not contribute anything to the effect of radiation trapping, and since this is the main interest for a singly doped crystal, the process can be turned off. Second, a simulation takes about ten times longer when this process is tuned on. Third, the results are very different when this process is turned on, and do not at all resemble the results from measurements, so something is wrong in the implementation or the model itself.

The energy migration in Yb is a competitive process to the fluorescence. In the simulation, every time a photon is absorbed there are two main events that can occur, see the flowchart in section 9, Fig.(9.2), fluorescence or energy transfer/migration. Every time a photon is transferred from one host to another in this process, it means that is is not emitted as fluorescence. When the lifetime is measured, this delay can be quite significant, and can thus increase the measured lifetime by a significant amount. This would imply that a high degree of energy migration could be seen in the measurements as it would increase lifetime. To test this, a series of lifetime measurements of the $^2F_{5/2}$ level in Yb were taken on a KYbW crystal. The KYbW crystal is a KYW crystal, where all Y atoms have been replaced by Yb atoms, i.e. a Yb100%:KYW. Since every Yb ion has a neighbour at every adjacent lattice point, the amount of energy migration would be a lot higher than in Yb5%:KYW. If this would reflect in a longer measured lifetime, the model implemented in the Monte Carlo simulation would be correct, otherwise it would have to be adjusted. The results of the measurements can be seen in Fig.(10.2)

The lifetimes obtained in the measurements are about a factor two higher than for the Yb5%:KYW, so at a first glance, lifetimes seemed to increase with the amount of energy transfer in the crystal. However, as doping concentration increases, so does radiation trapping; and at these very high concentrations the photon step size is very small, so the confocal microscopy set-up used might not reduce the radiation trapping nearly enough to see the true lifetimes. To investigate how much the set-up would reduce radiation trapping at this high concentration, a Monte Carlo simulation was run with the aperture diameter set to 2 mm and an Yb doping concentration of 100%. The resulting lifetime predicted by the simulation was 570 μs, very close to the measured lifetime of 500 μs. Thus, the long lifetime measured at high

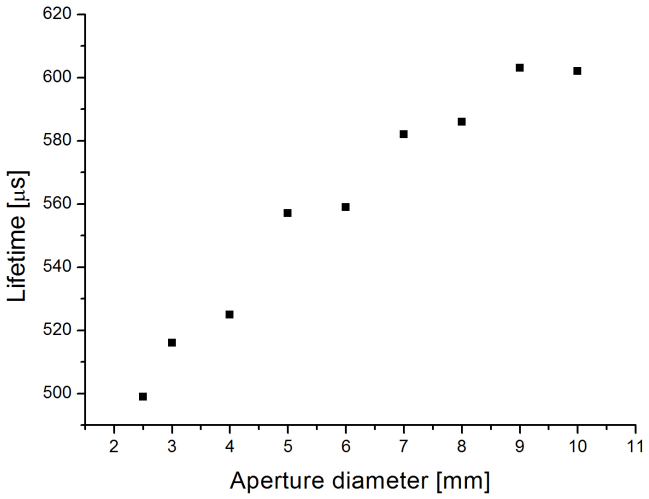

Figure 10.2. *A measurement series from the KYbW crystal.*

concentration is due to radiation trapping; it seems that the lifetime is not dependent on the amount of energy migration within the sample.

In order to properly simulate a co-doped crystal, the energy transfer/migration must be properly modeled to get reliable results, since this is the way energy is shared between the different ion species. Consequently, the Monte Carlo simulation cannot yet be applied to co-doped crystals.

Another possible source of error in the non-radiative energy model might be the values of the Förster radii, calculated in section 5. As mentioned there, an error in the calculated emission cross section in Er might result in a higher value of the Förster radii, which will result in erroneous outcomes in the simulations.

11 Summary and discussion

In this thesis, lifetimes measurements of Er and Yb doped crystals have been taken and analyzed. A method of reducing radiation trapping has been tested and evaluated, and a basic theory for explaining the results have been developed. Further, a Monte Carlo simulation has been constructed to simulate the processes of radiation trapping and non-radiative energy transfers, and to study their behaviour and effect on the crystals' lifetimes and transfer efficiencies from Yb to Er, in order to optimize doping concentrations. The most important results for each part will be summarized below.

11.1 A method of reducing radiation trapping

The method developed and analyzed in this thesis reduce the measured lifetimes with 10–40% depending on host crystal and doping concentration. The set-up for taking these measurements was relatively easy to build and works for practically any crystal. However, as the aperture diameter decreases, so does the signal to the detector, which means that it can be difficult to get reliable data for small apertures, or for crystals of low doping concentration where the fluorescence is weak to begin with. Also, care has to be taken when building the set-up so that the aperture sizes are in the right region, so that there will be any reduction of radiation trapping at all. If the apertures chosen are too large, there will be no difference in the measured lifetimes as the aperture diameter is changed, and the method will then not yield any results at all. The maximum aperture used in these measurements was 10 mm, and the magnification of the imaging system was a factor of 10, so the real maximum aperture size, was about 1 mm. If crystals with much higher doping concenrations are used, the apertures must be even smaller. The simplest way to achieve this is to increase the magnification of the imaging system.

By seeing the radiation trapping process as a random walk for the photons in the crystal, a simulation was constructed and compared to the measurements data. Using this approach it was possible to explain the behaviour of the results in a simple and yet effective way. Even though too many simplifications were made for any numerical predictions, the qualitative results were enough to suggest how to treat the measured data and approximate the true lifetime.

11.2 The Monte Carlo Simulation

By constructing a more complex and realistic model of the set-up, numerical predictions could be achieved. The Monte Carlo simulation had two main purposes, to simulate radiation trapping, and to simulate the redistribution of energy among the Yb and Er ions.

When simulating radiation trapping, the results from the Monte Carlo simulation were in fair agreement with the measurements taken, confirming the source and behaviour of the effect of the confocal microscopy set-up. When simulating the non-radiative energy transfer process however, the results were not so good. This is most likely due to an incomplete implementation of the processes at work.

11.3 Future work

To improve the accuracy of the simulation, both for radiation trapping and energy migration, further adjustments can be made.

11.3.1 Non-radiative energy transfers

By resolving the issues in this part of the simulation, a very handy way of studying the energy redistribution and transfer efficiencies between Er and Yb is obtained. Since the doping concentrations determine the efficiency of the laser output, it is of importance to know the optimum doping before building the laser. When simulating radiation trapping and the confocal microscopy set-up of reducing it, the number of photons simulated before 2000 detected photons was achieved could be as high as 7 000 000 for a crystal with low doping concentration and a small aperture. To run a simulation sequence where the aperture diameters range in 2–15 mm could take 16 hours. When simulating the non-radiative energy transfers, the radiation trapping can be turned off, and the aperture and detector as they are implemented in the simulation can be ignored. In order to detect 5000 photons it would only be necessary to trace 5000 photons, which takes a few seconds, so high accuracy is very easy to achieve when radiation trapping is ignored.

11.3.2 A finite beam size

The simulation assumes an infinitely narrow pump beam, instead of a gaussian beam. There are two ways of adjusting this. First, the photon starting positions could be randomly generated, within a normal distribution. This is simple to implement, but in order to get good results, the number of photons simulated must be increased quite a lot, so to get accurate results the simulations would take a lot longer to perform. The second option is to use the results from an infinitely narrow beam and adjust it in a proper way. The simulation results using a narrow beam can be seen as the impulse response for the system in question. The response for a system of a finite size beam can be obtained by convoluting the impulse response with the intensity profile of the beam in question [17]. Using this approach, the same number of photons can be traced for the same accuracy. There is one thing that must be changed if this approach is chosen. In order to use the convolution, the system must be linear and invariant. The system as it is

implemented is linear, but not invariant. That is, if the intensity of the beam is multiplied by a factor, the response will be multiplied by the same factor. It is not invariant, since a translation of the beam would result in a different response of the system, due to the finite size of the crystal. In order to utilize this method, the crystal would have to be infinitely wide, which is not difficult to change so it does not impose a great problem. There is a very good description of how to perform this calculation in an article by L. Yang and L. S. Jacques. [17]

References

[1] C. Nordling and J. Österman. *Physics handbook, 6th ed.* Studentlitteratur, Sweden, 2002.

[2] R. C. Hilborn. Einstein coefficients, cross sections, f values, dipole moments, and all that. *American Journal of Physics*, 50(11):982–986, 1982.

[3] William T. Silfvast. *Laser Fundamentals*. Cambridge University Press, New York, 1996.

[4] A. E. Siegman. *Lasers*. University Science, Mill Valley, Calif., 1986.

[5] S. Bjurshagen, J. E. Hellström, V. Pasiskevicius, M. C. Pujol, M. Aguiló, and F. Díaz. Fluorescence dynamics and rate equation analysis in Er^{3+} and Yb^{3+} doped double tungstates. *Applied Optics*, 45(19):4715 – 4725, 2006.

[6] J. A. Caird, A. J. Ramponi, and P. R. Staver. Quantum efficiency and excited-state relaxation dynamics in neodymium-doped phosphate laser glasses. *Journal of the Optical Society of America B*, 8(7):1391–1403, 1991.

[7] D. E. McCumber. Einstein relations connecting broadband emission and absorption spectra. *Physical Review*, 136(4A):954 – 957, 1964.

[8] R. S. Quimby. Range of validity of McCumber theory in relating absorption and emission cross sections. *Journal of applied physics*, 92(1):180–187, 2002.

[9] R. W. Boyd. *Nonlinear Optics*. Academic Press, Inc, San Diego, 1992.

[10] Stefan Bjurshagen. *Diode-pumped rare-earth-doped quasi-three-level laser*. PhD thesis, Department of Physics, Royal Institute of Technology, SE-106 91 Stockholm, Sweden, 2005.

[11] K. Petermann, D. Fagundes-Peters, J.Johannsen, M. Mond, V. Peters, J. J. Romero, S. Kutovoi, J. Speiser, and A. Giesen. Highly Yb-doped oxides for thin-disc lasers. *Journal of Crystal Growth*, 275(4A):135 – 140, 2005.

[12] V. E. Kisel, A. E. Troshind, V. G Shcherbitsky, and N. V. Kuleshov. Luminescence lifetime measurements in Yb^{3+}-doped $KY(WO_4)_2$ and $KGd(WO_4)_2$. In *Proceedings of ASSP*, 2004.

[13] L. H. Wang, S. L. Jacques, and L. Q. Zheng. MCML — Monte Carlo modeling of photon transport in multi-layered tissues. *Computer methods and programs in biomedicine*, 47(11):131–146, 1995.

[14] S. Torquato, B. Lu, and J. Rubinstein. Nearest-neighbor distribution functions in many-body systems. *Phys. Rev. A*, 41(4):2059–2075, Feb 1990.

[15] P. Hertz. Über den geigenseitigen durchschnittlichen Abstand von Punkten, die mit bekannter mittlerer Dichte im Raume angeordnet sind. *Mathematische Annalen*, 67:387–398, 1909.

[16] E. Hecht. *Optics, 4th ed.* Addison Wesley, San Francisco, 2002.

[17] L. Wang, S. L. Jacques, and L. Zheng. CONV - convolution for responses to a finite diameter photon beam incident on multi-layered tissues. *Computer Methods and Programs in Biomedicine*, 54(3):141 – 150, Nov 1997.